

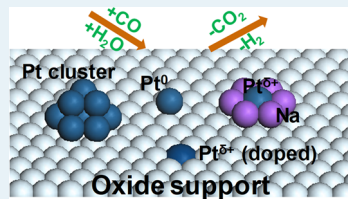
Understanding the Nature and Activity of Supported Platinum Catalysts for the Water–Gas Shift Reaction: From Metallic Nanoclusters to Alkali-Stabilized Single-Atom Cations

Salai Cheettu Ammal and Andreas Heyden*

Department of Chemical Engineering, University of South Carolina, 301 South Main Street, Columbia, South Carolina 29208, United States

Supporting Information

ABSTRACT: Identifying the nature of an active site and understanding the reaction mechanism at the atomic level are of critical importance in the design of efficient catalysts for targeted applications. While extended metal surfaces have been studied extensively for various catalytic processes and relative activities of different metals were predicted using volcano relationships, much less is known with regard to catalysis at metal/oxide interface sites. This Perspective focuses on recent computational studies that were aimed at understanding catalysis at such metal/oxide interface sites. The water–gas shift (WGS) reaction catalyzed by supported Pt catalysts has been chosen as a model system for such an analysis, since extensive computational studies with varying sizes of Pt clusters and supports are available and, thus, by comparison to experimental data, a deeper understanding of the active sites can be attained. Pt catalysts with different sizes and shapes stabilized on various supports were found to be active for the WGS. However, the identification of the exact nature and function of the active site in these catalysts is still a matter of debate. Here, we analyzed the computational studies performed using different active site models, namely, Pt surface models, reducible oxide supported Pt cluster models, and supported single Pt site models. The focus of this Perspective is not to summarize computational or experimental studies of the WGS but to highlight the importance of choosing appropriate active site models and methods in the computational studies such that the experimental behavior of these catalysts and the specific roles of the metal and support can be understood. Furthermore, results obtained for the WGS mechanism catalyzed by Na-stabilized single Pt cations supported on TiO₂ are discussed and the promotional role of alkali cations are identified. Finally, we touch upon the importance of uncertainty quantification to account for the inexact nature of DFT in the correlation of computational predictions with experimental observations.



KEYWORDS: supported Pt catalysts, alkali-stabilized Pt cation, water–gas shift, DFT, uncertainty quantification

1. INTRODUCTION

Heterogeneous catalysis is known to facilitate energy-efficient selective molecular transformations and will be a central science in driving the transition of chemicals and energy industries toward sustainability.¹ The design of novel active, selective, and stable catalytic processes that meet the needs of the present generation without compromising future generations is an important challenge for coming generations. Despite the fact that most industrial catalysts were identified using a trial-and-error approach, the rational design of heterogeneous catalysts is highly desirable. Unfortunately, rational design requires a deep understanding of the fundamental surface processes that are often still unknown. In recent years, computational catalysis has become a powerful tool in providing an atomistic picture of heterogeneous reactions, interpretation of spectroscopic data, elucidation of reaction mechanisms, and also for the prediction of the relative activity of materials that can be used in the design of novel catalysts.^{2–10} However, it is believed that the accuracy of currently used computational methods and models is still a bottleneck in establishing a truly predictive comprehensive theory of catalysis.¹¹

One of the main challenges in a computational catalysis study is to identify an accurate and computationally efficient active site model that can represent the catalyst present in a highly complex catalytic experiment. Various factors, such as size and shape of the metal active sites and the presence of supports and solvents must be taken into account in the design of an active site model. Simplified models are often used to describe heterogeneous catalytic systems that can realistically only provide correct predictions of experimental observations in cases where the contribution from the experimental reaction environment and the system complexity are minimal. For systems, where these contributions become important, reasonable predictions can be obtained only with a model that correctly accounts for the finer details in the chemistry of the catalytic system.¹¹ The next challenge in the correlation of computational results with the experimental data is the uncertainty that arises from the computational methods. Plane wave density functional theory (DFT) is commonly

Received: April 16, 2019

Revised: July 8, 2019

Published: July 12, 2019

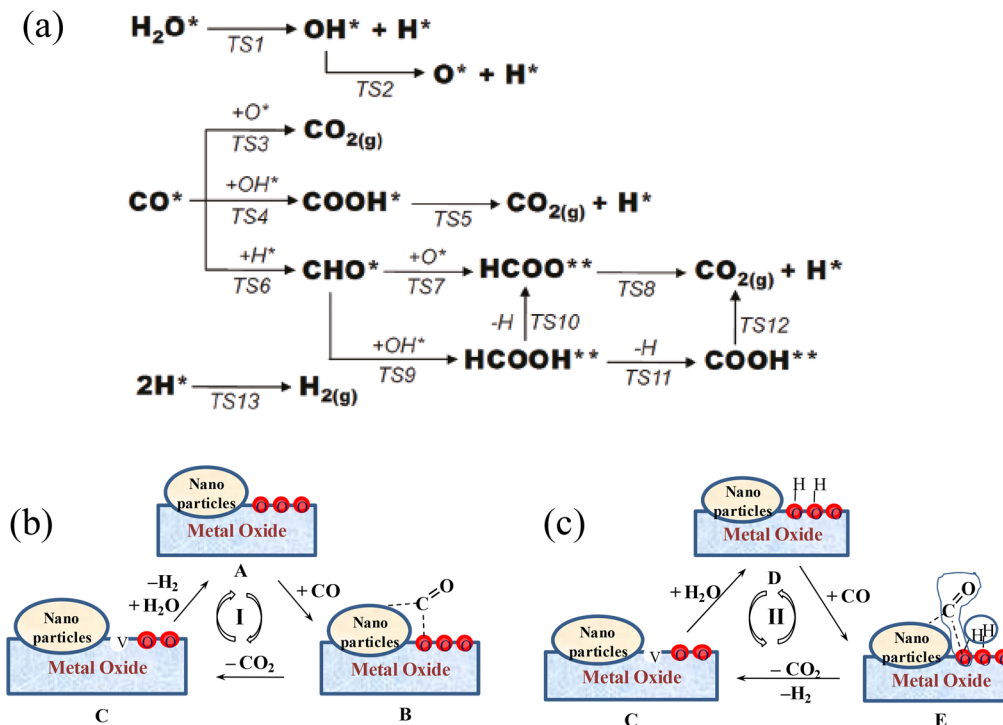


Figure 1. (a) Proposed reaction pathways of WGS on Pt metal surfaces. [Adapted with permission from ref 22. Copyright 2011, American Chemical Society, Washington, DC.] (b) Proposed redox pathway and (c) associative pathway with redox regeneration for the WGS at metal/oxide interface sites. [Adapted with permission from ref 55. Copyright 2013, Elsevier, Amsterdam.]

used to study heterogeneous catalytic reactions, since it is reasonably accurate and computationally efficient. However, in the case of bifunctional catalysts, which involve reducible oxide supports, such as CeO_2 , Fe_2O_3 , TiO_2 , etc., the standard DFT methods based on the generalized gradient approximation (GGA) fail to describe the electronic structure of the oxides, because of the well-known problem of the self-interaction error. Although the use of hybrid functionals can correct this deficiency, these methods are computationally not affordable for larger active site models. The DFT+U approach^{12,13} is another way to correct the self-interaction error; however, uncertainty still remains in choosing the U parameter for a specific system that can describe the correct electronic structure and, at the same time, yields reliable reaction enthalpies and activation barriers.¹⁴ Recent reports have addressed these problems using a Bayesian framework^{6,15–17} that can correlate computational predictions with experimental observations in the presence of these uncertainties to identify the active site structure. To understand how the computational models and methods used to study a specific catalyst system affect the correlation of computational predictions with experimental observations, we summarize here the computational studies of supported Pt catalysts for the water–gas shift (WGS) reaction.

The WGS, which can be described as



is an important industrial process that facilitates the removal of detrimental CO that formed as a side product from reforming or other catalytic processes, while maximizing the yield of H_2 , the most efficient and cleanest fuel. Since it is moderately exothermic, low CO levels can only be achieved at low temperatures while the kinetics is favored at higher temperature. Thus, a two-stage technology with a high-temperature

(350–500 °C) shift over a $\text{Fe}_2\text{O}_3/\text{Cr}_2\text{O}_3$ catalyst, followed by a low-temperature (200–250 °C) shift over a $\text{Cu}/\text{ZnO}/\text{Al}_2\text{O}_3$ catalyst, is currently used in industry.^{18–20} Although this technology is acceptable on an industrial scale, the development of an effective single-stage low-temperature WGS catalyst is still desirable for *in situ* hydrogen generation for automobile fuel cell applications. The ongoing research efforts on WGS catalysts can be classified into two categories. One research direction focuses on finding efficient alternative low-temperature WGS catalysts that can exhibit excellent activity as well as resistance to poisoning.^{21–23} In the second category, WGS is used as a probe reaction to understand the behavior and activity of newly developed catalysts.^{24,25} In both cases, supported Pt catalysts are one of the most widely studied catalysts for the WGS both experimentally and computationally, likely because Pt exhibits better performance, compared to other transition metals, and changes in activity by a few orders of magnitude can be achieved when it is supported on reducible oxides.^{21,22} Supported Au and Cu catalysts^{26–48} are the other candidates that have been investigated extensively for the low-temperature WGS. Here, we chose to analyze the computational studies of supported Pt catalysts since computational kinetic studies of the WGS are available for different active sites of Pt with identical levels of theory, such that a direct correlation with the experimental studies is possible.

Pt catalysts synthesized in various shapes and sizes (single atoms, nanoclusters, and nanoparticles) and supported on reducible/irreducible oxides, zeolites, carbon etc. were all found to be active for the WGS.^{20,23,24} Despite the rapid development of high-resolution characterization techniques that allow one to visualize single metal atoms or small metal clusters^{49,50} and also identify their coordination environment under reaction conditions,⁵¹ the determination of the exact active site for the WGS and operating reaction mechanism on

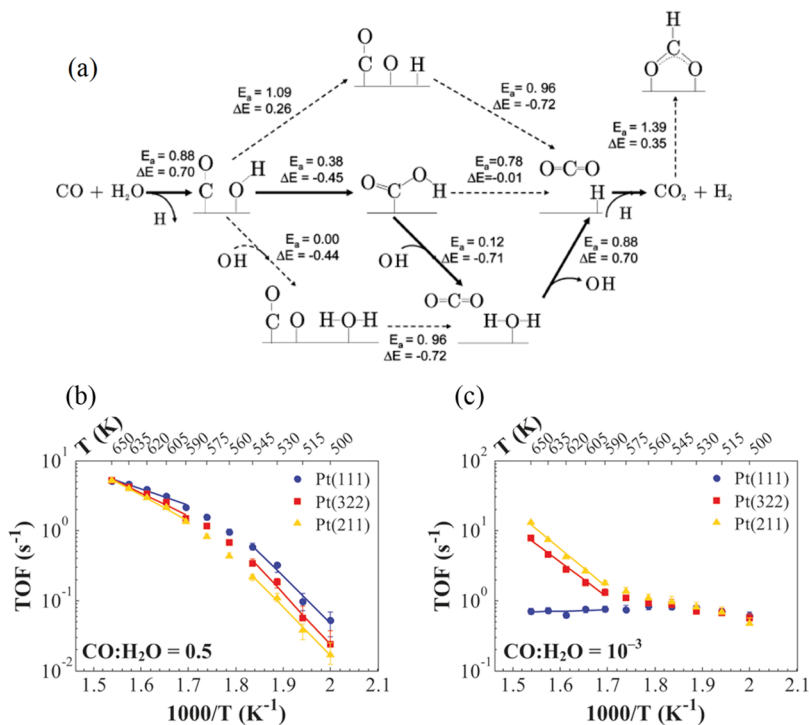


Figure 2. (a) Reaction network of possible WGS reaction steps on Pt(111). The numbers by the arrows indicate the forward activation energy barrier and the reaction enthalpy (in eV) for the corresponding elementary steps. [Adapted with permission from ref 56. Copyright 2008, American Chemical Society, Washington, DC.] (b, c) Turnover frequency (TOF) of WGS on Pt(111), Pt(211), and Pt(322) surfaces with different $CO:H_2O$ ratios. [Adapted with permission from ref 57. Copyright 2011. American Chemical Society, Washington, DC.]

these catalysts is still a matter of debate, because of the complex experimental catalyst system. In the case of supported Pt nanoclusters, experimental reports have claimed the active sites as Pt facets, corners, edges, or metal/support interface sites. When the nanoparticles can coexist with single Pt ions, disagreements have been reported regarding the active site being single Pt ions or small Pt nanoparticles. Computational studies with proper active site models could be very helpful here to acquire an atomic-level understanding of the active sites and reaction mechanism such that the activity of different sites can be compared and the limiting factors can be identified. The goal of this Perspective is to analyze recent developments in computational modeling of supported Pt catalysts and understanding the activity of interfacial metal sites for the WGS reaction. Specifically, we focus on understanding the activity of different Pt active sites, such as Pt surface sites and reducible oxide-supported Pt clusters, positively charged/neutral Pt atoms and alkali-stabilized single Pt cations for the WGS, and how computational predictions correlate with the experimental observations. The relevant experimental findings are also summarized in each section.

2. MODELING PLATINUM CATALYSTS FOR WGS

Understanding the activity of a heterogeneous catalyst for a specific reaction using computational techniques requires a multistep strategy so that the properties calculated at the microscopic scale (DFT calculations) can be related to experimental observables at the macroscopic scale (reactor scale).⁵² In the following, we summarize such a multistep approach used in the computational studies of supported Pt catalysts for the WGS. In the first step, a catalyst active site model is constructed based on available experimental data and an appropriate level of theory is chosen for the calculations.

The model structure is then refined by constrained ab initio thermodynamic analysis considering the reaction chemistry, composition, and experimental reaction conditions (temperature and partial pressure of gaseous species). Next, various elementary reactions of the proposed pathways are investigated and the reaction rate constants are calculated. A microkinetic analysis based on these DFT-derived parameters is then performed to obtain information regarding dominant reaction pathways, turnover frequencies (TOFs), reaction orders, and apparent activation barriers under experimental reaction conditions. The limiting factors such as rate-controlling elementary reaction and intermediates are identified using Campbell's degree of rate control and degree of thermodynamic rate control analyses or sensitivity analysis.^{53,54} Efforts have also been made to quantify uncertainties in elementary rate constants, because of errors in DFT energies, entropies, etc., and identify active sites through integration of computational and experimental data.

The reaction mechanism of the WGS on Pt metal surfaces^{21,22,56–60} is described based on a simple Langmuir–Hinshelwood process, where both reactants, CO and H_2O , adsorb on the metal surface followed by H_2O activation and dissociation (Figure 1a). In the redox pathway, CO is oxidized by atomic oxygen formed after two consecutive O–H bond dissociations of H_2O . In the associative pathways, only one O–H dissociation of H_2O is considered. CO can be oxidized by –OH, forming a carboxyl (–COOH) intermediate that undergoes further dissociation to produce CO_2 and adsorbed H. The formation of a formate (–HCOO) intermediate is also considered which involves multiple bond-forming and bond-breaking steps as described in Figure 1a. When the Pt metal is supported on a reducible-oxide, experimental studies have provided ample evidence^{61–67} that the oxygen atoms from the

Table 1. Kinetic Model Comparisons^a

	Pd(111)		Pt(111)	
	kinetic model	expt	kinetic model	expt
$\Delta H_{\text{ads}}^{\text{CO}}$ (eV)	-1.95	-0.66	-1.87	-0.66
r_{WGS} (s^{-1})	3.87×10^{-24}	1.93×10^{-10}	2.7×10^{-3}	1.19×10^{-20}
E_a (kJ mol ⁻¹)	441	190	404	154
CO order	-2.00	0.97	-2.00	0.98
H ₂ O order	1.00	1.00	1.00	1.00
CO ₂ order	0.00	0.00	0.00	0.00
H ₂ order	0.00	-1.50	-0.36	-1.49

^aAdapted with permission from ref 60. Copyright 2014, Elsevier, Amsterdam. Reaction conditions: $P = 1$ atm, $T = 553$ K, $y_{\text{CO}} = 6.8\%$, $y_{\text{CO}_2} = 8.5\%$, $y_{\text{H}_2\text{O}} = 21.9\%$, $y_{\text{H}_2} = 37.4\%$, balance inert. Experimental results from refs 68 and 79.

oxide supports are involved in the reaction mechanism. The proposed redox pathway at the metal/oxide interface (Figure 1b), also known as the Mars–van Krevelen mechanism, involves the oxidation of CO adsorbed on Pt by the oxygen of the oxide support, which creates an oxygen vacancy at the interface. The reduced support is then reoxidized by the activation of H₂O at the vacancy. In the presence of stable hydroxyl groups at the interface, associative pathways with redox regeneration (or -OH regeneration) are also proposed (Figure 1c) where carboxyl or formate intermediates are formed by the reaction of CO with surface -OH groups. In the following, we summarize the computational studies that used a multistep approach to investigate the WGS mechanism on supported/unsupported Pt catalysts and analyze their findings.

2.1. Platinum-Metal-Only Models. WGS activity measurements over reducible oxide-supported Pt catalysts clearly indicated that the support has a large influence on the activity. However, Pt nanoparticles supported on inert carbon or irreducible oxides, such as Al₂O₃, SiO₂, MgO, ZrO₂, etc. were also found to exhibit good activity for the low-temperature WGS, compared to the commercial WGS catalysts.^{58,68–75} Since these supports usually exhibit only a small promotional effect, the platinum metal alone is expected to be responsible for the observed WGS activity, and it has been shown that the active platinum remains in a metallic state, even in the presence of alkali additives in the case of the Pt/Al₂O₃ catalyst.⁷⁰ Hence, computational studies have used unsupported Pt surface models to understand the mechanism of the WGS and develop kinetic models. Grabow et al.⁵⁶ reported the first DFT-based multistep approach to investigate the WGS reaction on a Pt(111) surface model and compared the results to experimental data measured for an alumina-supported Pt catalyst (Pt/Al₂O₃). A total of 17 elementary steps representing the redox, carboxyl, and formate pathways (Figure 2a) were investigated using DFT and a mean-field microkinetic model.^{76,77} After introducing a coverage-dependent CO binding energy and adjusting some of the kinetic parameters, a good agreement of DFT predictions with the experimental data was obtained. The microkinetic model suggested that the CO surface coverage is ~2/3 ML (where ML denotes monolayer), the mechanism follows a carboxyl pathway, and formate species are only spectator species. The rate-limiting step was identified as the direct decomposition of COOH to CO₂ and H. Although the reaction of COOH with OH to form CO₂ and H₂O seemed to be highly favorable, this path was found to be limited, because of the low surface coverage of OH under reaction conditions. It was suggested that an increased

amount of H₂O could promote the reaction of COOH + OH and thus increase the rate. Note that a good agreement with the experimentally measured rates and reaction orders was obtained only with the fitted model parameters (reaction energies and barriers of many steps were modified by at least 0.30 eV), suggesting that the steps/defects of Pt nanoclusters could also play a role in this reaction.

In a later study, Stamatakis et al.⁵⁷ investigated the contribution of different site types—namely, steps and terraces—on the overall WGS activity through DFT and kinetic Monte Carlo (kMC)⁷⁸ simulations over (111), (211), and (322) surfaces of Pt. Under industrially relevant conditions, their kMC analysis revealed similar rates for all three surfaces and concluded that the WGS reaction is structure-insensitive, as far as the metal sites are concerned (Figure 2b). Here again, the carboxyl pathway was found to be favorable; however, the rate-limiting step on the terrace sites appeared to be the carboxyl formation process rather than the carboxyl dissociation process, as reported by Grabow et al.⁵⁶ Further analysis revealed that the WGS chemistry does become structure-sensitive when CO:H₂O ratios are on the order of 10⁻³ or lower (see Figure 2c) and the dominant pathway follows the redox mechanism at the step sites. It was concluded that different sites, such as steps, terraces, or terrace/step interfacial sites, contribute through different elementary processes to the overall rate and the contribution of each site varies with operating conditions.

Clay et al.⁶⁰ also investigated the WGS mechanism on a Pt(111) surface model with the aim of comparing the intrinsic WGS activity of Pt and Pd catalysts. Their analysis included an additional pathway for the concerted formation of carboxyl from CO and H₂O. An analytical kinetic model developed in analogy to an electrical circuit analysis⁸⁰ revealed that the carboxyl pathway is preferred on both metals and the intrinsic rate on Pt is higher than on Pd. The baseline model predicted unphysically low absolute rates, because of a high coverage of CO, and further suggested that the water dissociation is the rate-controlling process. The inclusion of a coverage-dependent CO binding energy in the analysis was found to yield reasonable rates and shifted the rate-controlling step to the carboxyl formation process. Comparison of the calculated kinetic parameters with the experimental data obtained for Pd/ γ -Al₂O₃ and Pt/ γ -Al₂O₃ catalysts revealed that the calculated reaction orders and apparent activation energies are not consistent with the experimental data (Table 1). Although computations correctly predicted the experimentally observed relative order of activity between Pt and Pd catalysts, the failure to recover experimentally observed reaction orders and

activation barriers suggested that even a nominally inert support, such as Al_2O_3 , could play an active role in the WGS activity and that the metal-alone model may not be sufficient to reproduce experimental observations. In another recent study,⁸¹ Williams et al. have used linear scaling and Brønsted–Evans–Polyani (BEP) relations to analyze the trends in the reactivity of transition metals for the low-temperature WGS reaction. The ability of metals to form O–CO bonds, as determined from the oxygen binding energy and the coverage of CO on the metals, were found to be the important parameters that control the rates for the WGS reaction. Based on this analysis, it was proposed that a maximum turnover frequency for the WGS can be achieved on catalysts that combine metals that adsorb O weakly, such as Au clusters or Pt nanoparticles, with supports that are capable of easily dissociating water. This analysis further implies that the WGS mechanism on supported metal catalysts is bifunctional and the inclusion of the support in the analysis is very important.

2.2. $\text{Pt}_n/\text{Oxide Interface Models}$. Over the last two decades, many experimental studies reported that Pt nanoparticles supported on reducible oxides, such as CeO_2 , TiO_2 , FeO_x , and the mixed oxides, are active for the low-temperature WGS^{45,61,64,69,75,82–91} and among them TiO_2 - and CeO_2 -based Pt catalysts are currently the front runners for fuel cell applications. These studies have provided strong evidence that the support plays a vital role in the WGS mechanism. Since formate intermediates were observed during the WGS on Pt catalysts supported on reducible oxides, earlier experimental studies suggested that the WGS reaction occurs via a formate mechanism.^{83–85,92} However, latter experimental studies on Pt/TiO_2 and Pt/CeO_2 catalysts provided strong support for the redox mechanism and suggested that the observed formate and carbonate surface species should be considered as inactive spectator species for the steady-state WGS reaction.^{61,63,64,68,93,94} While only the redox mechanism was proposed for the WGS on Pt/TiO_2 catalysts, both the redox and associative formate with –OH group regeneration mechanisms were proposed for the Pt/CeO_2 catalyst.^{61,94} Furthermore, it has been shown that the Pt/TiO_2 catalysts are more active than the Pt/CeO_2 catalysts.^{61,67,93,95} A recent study on examining the size effects of Pt supported on FeO_x for the WGS reaction suggested that the redox mechanism with a sequential production of H_2 and CO_2 operates on Pt single atoms whereas the associative formate mechanism in which H_2O is activated on the FeO_x surface operates on the Pt nanoparticles.⁹¹ It is currently a well-accepted fact that the reducible-oxide-supported noble-metal catalysts are bifunctional in that the metal adsorbs/activates CO and the oxide support activates H_2O . It is also believed that the WGS activity of the catalyst is influenced by the redox properties of the support oxide such as reducibility, high oxygen mobility, and particularly the formation of hydroxyl groups in close proximity to the metal.

Similar to the reducible oxide supports, transition-metal carbides were also proposed as promising catalyst supports, because of their ability to activate H_2O . Recent experimental studies revealed that Mo_2C supported Pt nanoparticles exhibited an enhanced performance for the WGS, relative to their oxide-supported counterparts.^{96–101} The active sites in these catalysts were suggested to be Pt–Mo alloy nanoparticles that are in contact with the Mo_2C support;⁹⁶ however, the mechanism of the WGS and the origin of the enhanced activity

of these catalysts is not well understood. A recent computational study¹⁰² examined the WGS mechanism on a Pt monolayer supported on $\text{TiC}(001)$ and suggested that the reaction follows a carboxyl mechanism rather than a redox mechanism. Based on the comparison of activation barriers and rate constants of individual elementary reactions, this study claimed that the $\text{Pt}_{\text{ML}}/\text{TiC}(001)$ is a highly active catalyst, compared to $\text{Pt}(111)$ and Pt_n/CeO_2 catalysts due to favorable H_2O and COOH dissociation on the $\text{Pt}_{\text{ML}}/\text{TiC}(001)$ surface. It was further suggested that the $\text{Pt}_{\text{ML}}/\text{TiC}(001)$ system exhibits a much lower density of Pt 5d states near the Fermi level, compared to that of $\text{Pt}(111)$, because of the electronic perturbation of Pt atoms when in contact with $\text{TiC}(001)$ that would strongly improve its WGS activity. However, these results also indicate that the monolayer Pt supported on $\text{TiC}(001)$ adsorbs CO ($E_{\text{ads}} = -2.47$ eV) and other intermediates much stronger than the $\text{Pt}(111)$ surface and the effect of CO coverage as well as the availability of empty sites for the WGS reaction are not considered in this study. Although experimental studies have shown that the metal-carbide-supported Pt catalysts exhibit better performance for the WGS, compared to the oxide-supported Pt catalysts, more computational and experimental studies are necessary to appropriately attribute the cause for the apparent superior performance. Even in the case of well-studied oxide supported Pt catalysts, the exact nature and function of the Pt active site, the role of the support, and the reaction mechanism are still under debate. The experimental studies discussed above indicate that the WGS mechanism and activity could change with the support used and the size of the Pt particles. Thus, the mechanism for each catalyst system must be analyzed in order to understand the individual role of the support and metal particle. Computational studies of the WGS on Pt clusters supported on TiO_2 and CeO_2 have tried to resolve these issues and obtained a molecular level understanding of each component at the metal/oxide interface sites.^{55,87,89,103–105} Note that only very few computational studies have yet been reported that used the multistep approach to investigate the complete catalytic cycles of the WGS at Pt_n/oxide interface sites and calculated the kinetic parameters that are comparable to experimental data.^{55,103–105}

Activation of H_2O is an important process in the WGS mechanism and is a common step in both the redox and associative pathways. Since earlier studies on various metals and metal/oxide interfaces proposed H_2O dissociation as a rate-controlling process for the WGS,^{27,30,33,61,106–108} a few theoretical studies also examined this process on CeO_2 -supported Pt clusters. Bruix et al.⁸⁷ performed DFT calculations to investigate the dissociation of H_2O on $\text{Pt}(111)$, on free Pt_{79} and Pt_8 cluster models, and at the interface of a Pt_8 cluster supported on CeO_2 , to understand the effect of corner/edge Pt atoms with smaller coordination numbers and the presence of support on H_2O activation. Except on $\text{Pt}(111)$, the first O–H dissociation of H_2O was found to be exothermic on all the Pt clusters with the reaction energy being -1.3 eV on the supported cluster. A net $\text{Pt} \rightarrow \text{CeO}_2$ charge transfer was observed for the Pt_8/CeO_2 system and it was suggested that the metal cluster appears as a fluxional system that can change geometry and charge distribution to allow for better accommodation of adsorbates. Comparing these DFT results with their valence photo-emission experiments, the authors concluded that the admetal \leftrightarrow oxide electronic interactions significantly enhance

the catalytic activity of Pt and the activity increases in the following order: $\text{Pt}(111) \ll \text{Pt}/\text{CeO}_2(111) < \text{Pt}/\text{CeO}_x/\text{TiO}_2(110)$. However, it is noteworthy that even on the CeO_2 -supported Pt clusters, H_2O dissociation was investigated only on the Pt clusters and the possibility of the presence of oxygen vacancies at the interface and the activation of H_2O on these vacancies are not considered in this work. Vecchietti et al.⁸⁸ later considered these possibilities by examining the stability of oxygen vacancies and their reaction with H_2O at the interface of a Pt_8 cluster supported on CeO_2 and Ga-doped CeO_2 (CeGa). Atomistic thermodynamic analysis suggested that (i) these systems present a high degree of reduction under WGS reaction conditions and (ii) the Pt/CeGa system will exhibit 2–3 times more oxygen vacancies than the $\text{Pt}-\text{CeO}_2$ system. The H_2O dissociation process on these vacancies were investigated by calculating only the intermediates and it was found that the adsorption and activation of H_2O on the oxygen vacancies are highly favorable compared to those on the Pt clusters. Both experimental observations and DFT calculations provided evidence that the oxygen vacancy filling by H_2O is always fast in either Pt/CeO_2 or Pt/CeGa systems, suggesting that the H_2O activation is not the rate-limiting process for the WGS in CeO_2 -based systems.

In a series of articles published in the past few years, we reported complete mechanistic and kinetic studies of the WGS at the interface sites of Pt_n clusters supported on $\text{TiO}_2(110)$ and $\text{CeO}_2(111)$. The $\text{Pt}_8/\text{TiO}_2(110)$ and $\text{Pt}_{10}/\text{CeO}_{2-x}(111)$ interface models (Figure 3) used for the mechanistic study

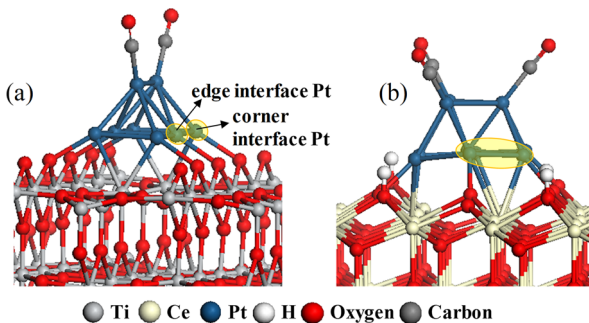


Figure 3. (a) $\text{Pt}/\text{TiO}_2(110)$ catalyst model used to study the WGS reaction mechanism. [Adapted with permission from ref 55. Copyright 2013, Elsevier, Amsterdam.] (b) $\text{Pt}/\text{CeO}_2(111)$ catalyst model used for the investigation of the WGS reaction mechanism. [Adapted with permission from ref 105. Copyright 2014, Elsevier, Amsterdam.] The highlighted areas correspond to the interfacial Pt active sites considered in these works.

were chosen based on constrained ab initio thermodynamics analysis performed on small Pt clusters supported on $\text{TiO}_2(110)$ ¹⁰⁹ and $\text{CeO}_2(111)$ ¹¹⁰ under WGS reaction conditions. The Pt cluster size was chosen based on the convergence of the interface oxygen vacancy formation energy, with respect to the Pt cluster size, which suggested the presence of multiple oxygen vacancies at the interface of $\text{Pt}_{10}/\text{CeO}_2$, whereas no oxygen vacancy was found to be stable at the Pt_8/TiO_2 interface under WGS reaction conditions. Further analysis revealed that the noninterfacial Pt atoms of both the Pt_8/TiO_2 and $\text{Pt}_{10}/\text{CeO}_{2-x}$ models are likely covered/poisoned by CO due to strong adsorption of CO on these sites and that the surface hydroxyl formation is favorable only on the $\text{Pt}_{10}/\text{CeO}_{2-x}$ model.

Different pathways of the WGS reaction have been examined at two different sites of the $\text{Pt}_8/\text{TiO}_2(110)$ model, namely, edge interface Pt⁵⁵ and corner interface Pt¹⁰³ (Figure 3a), using the PBE functional and microkinetic models were developed that are based solely on the parameters calculated by DFT and harmonic transition state theory (no fitting parameters were used). The kinetic analysis of these pathways at the edge interface Pt site (Figure 4) suggested the following:

- (1) A CO-promoted redox pathway dominates at lower temperature (473–623 K) and the classical redox pathway becomes dominant at temperatures above 673 K;
- (2) the associative pathways are less favorable, compared to redox pathways;
- (3) H_2O dissociation and H-diffusion both occur on the TiO_2 support and are rate-controlling, in agreement with the mass spectrometry experiments performed by Kalamaras et al.;⁶³ and
- (4) calculated apparent activation barriers (0.46–0.58 eV) and reaction orders at different reaction conditions were in good agreement with experimental data.^{63,70,93}

A higher turnover frequency (TOF) and lower apparent activation barrier were observed for the edge interface Pt site, compared to the previously reported $\text{Pt}(111)$ surface sites, which was attributed to the presence of a unique metal/oxide interface site at the three-phase boundary of Pt_8/TiO_2 with the metal exhibiting a reduced CO adsorption strength and the oxide providing vacancy sites that facilitate H_2O dissociation. On the corner interface Pt sites, the redox pathway was again found to be dominant, compared to the associative pathways, whereas the calculated TOFs were ~2 orders of magnitude lower than that of the edge site at temperatures below 523 K, because of the slightly stronger adsorption of CO at the corner Pt site, compared to the edge interface Pt site.

On the $\text{Pt}_{10}/\text{CeO}_2(111)$ model, the WGS mechanism was investigated at the interface site depicted in Figure 3b by examining the redox pathway, associative pathway, and the associative pathway with redox regeneration route using the PBE+U methodology.^{104,105} Explicit consideration of additional CO and H atoms was found to be necessary in order to obtain reasonable TOFs and apparent activation barriers. Both redox and “associative carboxyl with redox regeneration” pathways seem to contribute to the overall rate, while the dominant contribution comes from the latter pathway (Figure 5).¹⁰⁵ It was shown in a later study that the associative carboxyl pathway (that does not include the oxygen vacancy formation at the interface) is not a dominant pathway for this catalyst system, even though non-negligible rates were predicted for a CO-assisted associative carboxyl pathway.¹⁰⁴ Although the $\text{Pt}/\text{CeO}_2(111)$ model predicted higher TOFs of the WGS, compared to the reported platinum-metal-only models, the calculated TOFs were slightly lower and activation barriers were higher for the $\text{Pt}/\text{CeO}_2(111)$ model, compared to the $\text{Pt}/\text{TiO}_2(110)$ model, which is a trend that is also observed experimentally.⁹³ Two parameters were identified to be critical for understanding the observed activity trends, namely, the CO adsorption strength of interface Pt and the stability of the oxygen vacancy at the interface oxide site. The lower TOF observed for the $\text{Pt}/\text{CeO}_2(111)$ catalyst was explained by the availability of fewer active Pt sites at the interface due to strong adsorption of CO ($E^{\text{ads}} > 2$ eV), whereas nearly all interfacial Pt atoms of the $\text{Pt}/\text{TiO}_2(110)$ catalyst could be active, because

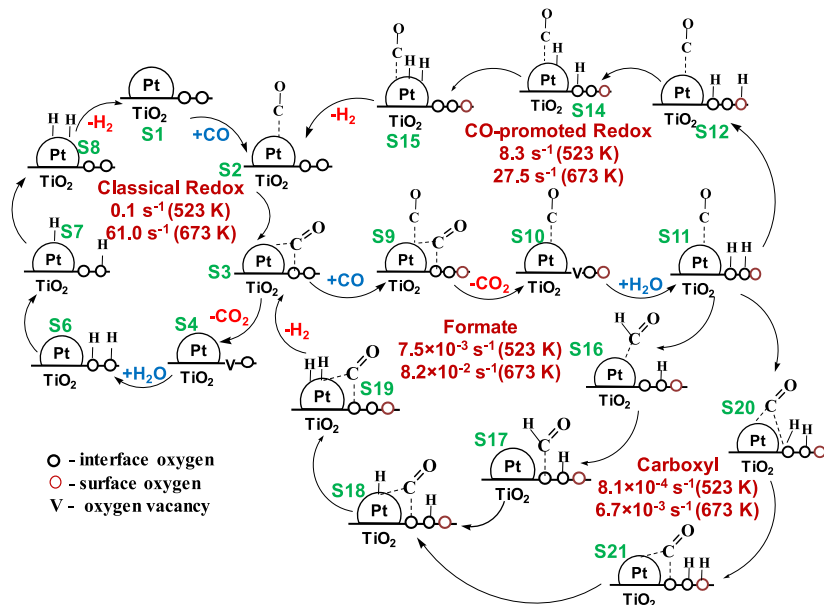


Figure 4. Reaction network of possible WGS reaction steps at the edge interface Pt of Pt/TiO₂ model. The numbers provided for each pathway are the overall rates (in s⁻¹) calculated at two representative temperatures ($P_{CO} = 0.1$ atm, $P_{H_2O} = 0.2$ atm, $P_{CO_2} = 0.1$ atm, $P_{H_2} = 0.4$ atm). [Adapted with permission from ref 55. Copyright 2013, Elsevier, Amsterdam.]

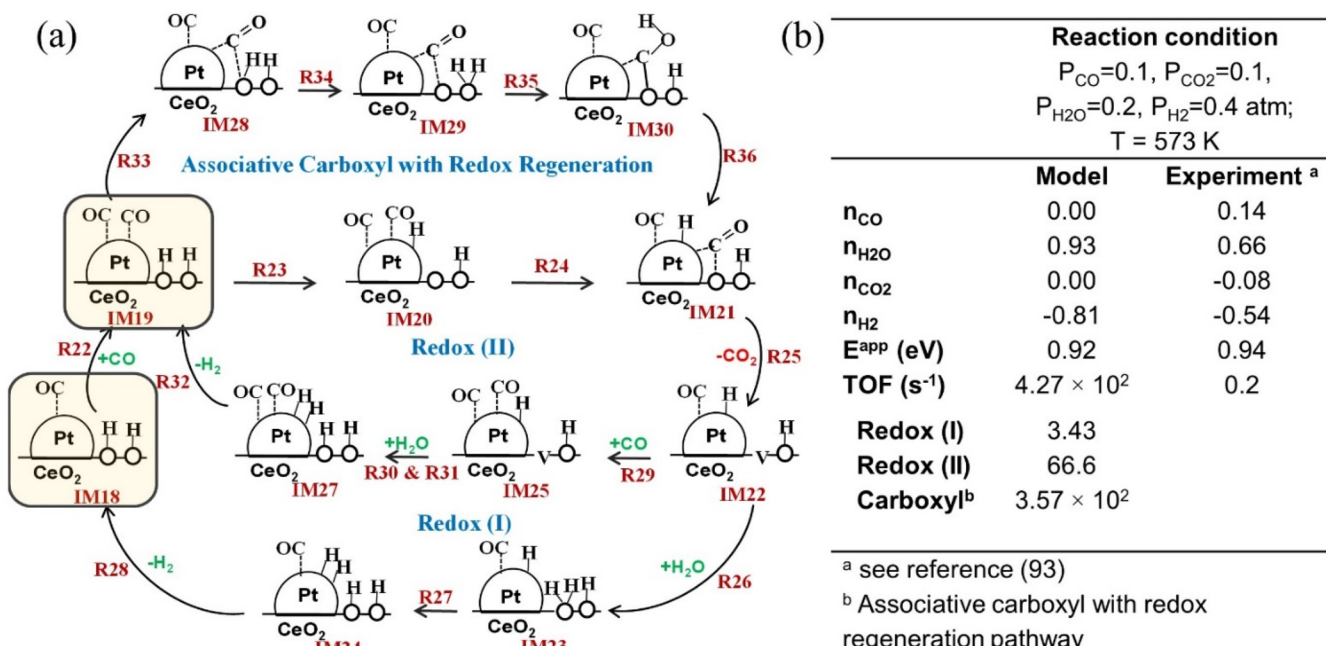


Figure 5. (a) Network of possible CO- and H-assisted WGS reaction steps at the TPB of Pt/CeO₂(111). (b) Reaction orders (n_i), apparent activation energies (E^{app}), and turnover frequencies (TOF) calculated from microkinetic models. [Adapted with permission from ref 105. Copyright 2013, Elsevier, Amsterdam.]

of a weaker CO adsorption ($E^{ads} < 1$ eV) on these sites. The higher activation barrier predicted for the Pt/CeO₂ catalyst was attributed to a very stable oxygen vacancy structure that is involved in the catalytic cycle of Pt/CeO₂, compared to that of the Pt/TiO₂ catalyst system. It was further suggested that the WGS activity of these catalysts can be improved by modifying these two parameters. Since the thermodynamic analysis predicted that the oxygen vacancy formation energy at the interface of the chosen Pt clusters is converged, with respect to the cluster size, and increasing the Pt cluster size is not going

to affect either the oxygen vacancy formation energy or the CO adsorption energy at the interface, it is believed that the Pt₈/TiO₂(110) and Pt₁₀/CeO_{2-x}(111) models used in these studies can represent the interface of TiO₂- and CeO₂-supported Pt nanoparticles typically used in experimental studies. These analyses clearly manifest the benefits of computational modeling for attaining an atomic level understanding of the reaction mechanism and in guiding the correct interpretation of experimental observations.

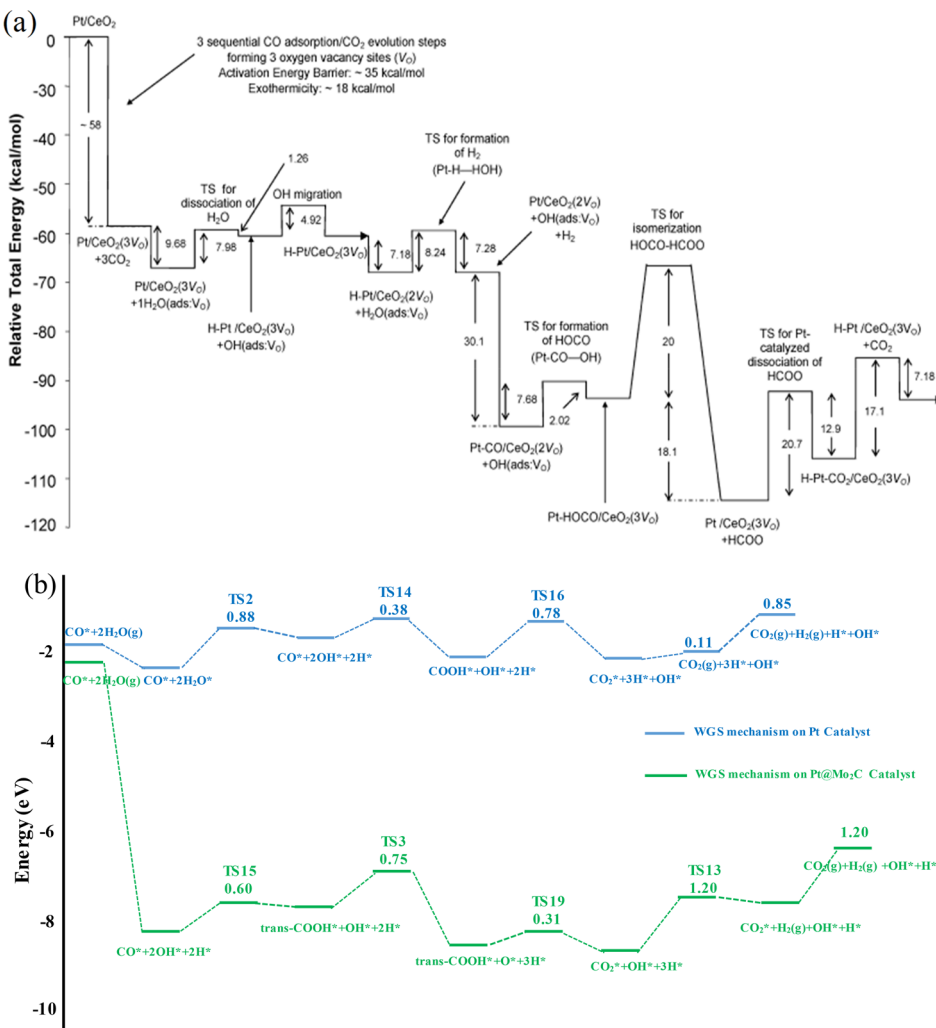


Figure 6. (a) Complete energy diagram for the WGS reaction after the depletion of all active oxygen atoms surrounding the platinum atom on a Pt-doped CeO₂(111) model. [Adapted with permission from ref 120. Copyright 2009, American Chemical Society, Washington, DC.] (b) Calculated potential energy diagram for the WGS reaction on the Pt(111) surface (blue line) and Pt@Mo₂C(001) surface (green line). [Adapted with permission from ref 133. Copyright 2017, The Royal Society of Chemistry, London.]

2.3. Supported Single Pt Atom Models. In recent years, there is an explosive growth in research on supported single-atom catalysts, because they offer fascinating prospects, such as significant catalyst cost reduction by maximizing the efficient utility of expensive noble metals, and high activity and selectivity toward various heterogeneous reactions. Recent reviews summarized the advances in successful synthesis and characterization of these single-atom catalysts and their catalytic performance toward various reactions.^{25,111–117} In addition, different types of supported single-atom catalysts were also examined computationally to understand the nature of metal–support interaction and the reaction mechanisms.^{118–137} Here, we focus on the experimental and computational studies of supported Pt single-atom catalysts for the WGS. Madras and co-workers have synthesized nanosized Pt single-atom catalysts a decade ago where Pt ions are substituted in the 2+ state in TiO₂, CeO₂, and Ce_{1-x}Ti_xO_{2-δ}.^{138,139} The WGS activity measurements on these catalysts revealed a high activity and low activation energy for the Pt²⁺-doped TiO₂ and it was found to be not deactivated by carbonate formation.

Flytzani-Stephanopoulos and co-workers first proposed the positively charged isolated metal ions supported on oxides as active species for the WGS in 2003, when they discovered that the performance of conventional Au/CeO₂ and Pt/CeO₂ catalysts remain unaffected after chemically leaching out the metallic nanoparticles and characterization of the leached catalysts confirmed the presence of isolated metal cations.³⁴ In the later reports, this research group has further demonstrated that atomically dispersed Pt stabilized by alkali ions and supported on various oxides, zeolites, and carbon supports are all active for the WGS reaction, leading them to claim that a common single-site species exists in the different catalysts that is responsible for the WGS activity.^{24,140–143} In another recent study, Chen et al. demonstrated that the activation energy for the WGS reaction decreases with downsizing of the Pt species supported on FeO_x, and the single Pt atoms exhibited a lower activation energy and higher activity for the WGS, compared to the Pt nanoparticles.⁹¹ These claims were contradicted by an experimental report by Ding et al., who used infrared (IR) spectroscopy with CO as a probe molecule to investigate the activity of supported single Pt atoms and nanoparticles for the low-temperature CO oxidation and WGS reaction.⁷⁵ Based on

the observation that only the CO IR peak related to the Pt nanoparticles disappeared during WGS and the Pt single atom related CO IR peaks remained unaffected, these authors claimed that the nanoparticles are the active species for the WGS, whereas the single Pt atoms are only spectators. Such contradictory predictions/interpretations of experimental findings further emphasize the importance of obtaining a molecular level understanding of the active site and reaction mechanism to confirm the interpretation of experimental observations.

One might intuitively assume that computational modeling of a supported single-atom catalyst is very much simplified, because of the presence of a single metal atom, compared to a metal nanoparticle or cluster. However, modeling of the support surface and identifying the stable location and nature of the active metal atom on the support still poses a major challenge. DFT calculations that investigated the CO oxidation mechanism on Pt_1/FeO_x catalysts identified that the anchoring site of the Pt atom is the 3-fold hollow site on the O₃-terminated $\text{Fe}_2\text{O}_3(001)$ surface and that the Pt atom is positively charged, because of significant charge transfer from the Pt metal to the iron-oxide surface.^{118,129} Bruix et al. used a $\text{Ce}_{40}\text{O}_{80}$ nanoparticle as a representative model for nanostructured ceria and identified a specific structural element, a ceria “nanopacket”, as anchoring site for a Pt^{2+} ion in their DFT calculations.¹²² The nanoparticle features a truncated octahedral shape with very small O-terminated {100} nanofacets on which Pt adsorbs strongly, acquiring a square-planar coordination and a 2+ oxidation state. Further analysis predicted that the Pt^{2+} ion located inside the square pocket of O²⁻ ions is very stable, such that it could resist aggregation and diffusion into metallic Pt nanoparticles. In another study, methanol steam reforming was examined on $\text{Pt}_1(\text{Au}_1)/\text{ZnO}$ catalysts and the calculations predicted that the cationic Pt or Au atoms anchored onto the surface Zn vacancy positions are thermodynamically stable and resistant to segregation and agglomeration during synthesis and the catalytic cycle.¹¹⁹ In a recent study, Thang et al. explored the atomistic nature of the isolated Pt species supported on anatase TiO₂ by comparing DFT calculated adsorption energies and stretching frequencies of Pt-adsorbed CO with experimental reports.¹³⁵ The Pt atom adsorption on the TiO₂(101) surface was considered through five different models, including a single Pt atom, a PtO unit, a PtO₂ unit, and substitution of surface Ti and O by Pt. By comparing the calculated absolute values and the shifts of vibrational modes of CO adsorbed on these sites with the experimental values for the isolated Pt species, the authors assigned the structure of experimentally observed single Pt species to the adsorbed PtO₂ unit that exhibits a 2+ oxidation state for Pt. These studies confirm that the single Pt atoms stabilized on various oxides are positively charged and are active for various reactions. However, only very few computational studies attempted to investigate the WGS mechanism on these supported single Pt sites and understand their activity.

Kinch et al.¹²⁰ used a Pt-doped CeO₂(111) model in which the Pt atom is binding to a surface Ce vacancy to investigate the WGS mechanism. They considered both the redox and formate pathways. A small cluster of $\text{Ce}_{24}\text{O}_{36}$ was used to model the ceria support and the calculations were performed using the standard DFT method with PBE functional. Based on the reaction energies and barriers (Figure 6a), the authors suggested that the redox pathway is favorable with elementary reaction barriers of only 8–12 kcal/mol. Also, formate species

appear to play a role in the formation of H₂. Since an initial thermodynamic analysis was not performed to identify a suitable model for this system, the oxidation of CO by lattice oxygen was found to be highly exothermic and a kinetic analysis of this pathway would most likely result in very low rates. In addition, it has long been demonstrated that the description of rare-earth oxides, such as ceria, with standard DFT methods leads to the wrong electronic structures¹⁴ and it is now a common practice to use DFT+U or hybrid methods to circumvent this problem.

In another study, Li et al.¹³³ investigated the mechanism of the WGS on a Pt-doped Mo₂C surface model (a Mo atom on the Mo-terminated $\beta\text{-Mo}_2\text{C}(001)$ surface was replaced by Pt) using DFT methods with the PBE functional. Comparison of elementary reaction energies, activation barriers, and rate constants suggested that the carboxyl mechanism is more favorable than the redox and formate mechanisms for this system. The calculations revealed that all species involved in the WGS prefer to interact with the Mo atoms rather than the Pt atom and the role of Pt is to facilitate H₂ production. The enhanced adsorption of small species on the Mo sites inhibits the formation and desorption of CO₂, even in the presence of platinum. The energetics of the WGS shown in Figure 6b clearly suggests that the surface Mo atoms will be occupied by O atoms under WGS conditions and a catalytic cycle to regenerate the active site is likely not possible with the chosen model. This again emphasizes the importance of performing a proper thermodynamic analysis to identify a suitable active site model that could be present under WGS conditions and that can predict the experimentally observed good activity for the Pt/Mo₂C catalyst.

In our recent reports,^{136,137} the WGS mechanism was investigated on atomically dispersed Pt supported on a TiO₂(110) surface using DFT and microkinetic modeling. A constrained thermodynamic analysis was initially performed to identify the stable location of the Pt atom on the TiO₂(110) surface. This study suggested that the Pt²⁺-doped TiO₂ surface with additional H atoms adsorbed on surface O atoms is the most stable surface at temperatures of <500 K in the presence of a reducing H₂/H₂O atmosphere. Further analysis of these models under experimental WGS conditions (H₂/H₂O/CO atmosphere; see Figure 7) indicated that the TiO₂-supported single Pt atoms adsorb CO strongly ($E_{\text{CO}}^{\text{ads}} = -2.0$ to -3.5 eV) and that a CO and H-adsorbed Pt²⁺-doped TiO₂ surface (Figure 7c) is still the most stable structure at low temperatures and a structure with Pt-CO unit adsorbed on a stoichiometric TiO₂ surface (nondoped, Figure 7d) becomes more stable at temperatures of >300 K. Bader charge analysis confirmed that the doped structure has a Pt²⁺ ion ($Q_{\text{Pt}} = +0.75$) with a square planar structure and the Pt atom in the nondoped structure is also slightly positively charged ($Q_{\text{Pt}} = +0.30$) due to back-donation of electrons from Pt to CO. The WGS mechanism was examined on the doped model considering the redox and associative carboxyl/formate with redox regeneration pathways.¹³⁷ Only the redox pathway was considered for the nondoped model, because the surface –OH species are not stable in this structure.¹³⁶

The reaction rates calculated using a DFT-based microkinetic model suggested that the redox pathway is dominant for the doped surface model and the formate pathway also contributes significantly at temperatures below 573 K. Calculated TOFs (see Table 2) confirm that the single Pt sites present in both the doped and nondoped models can

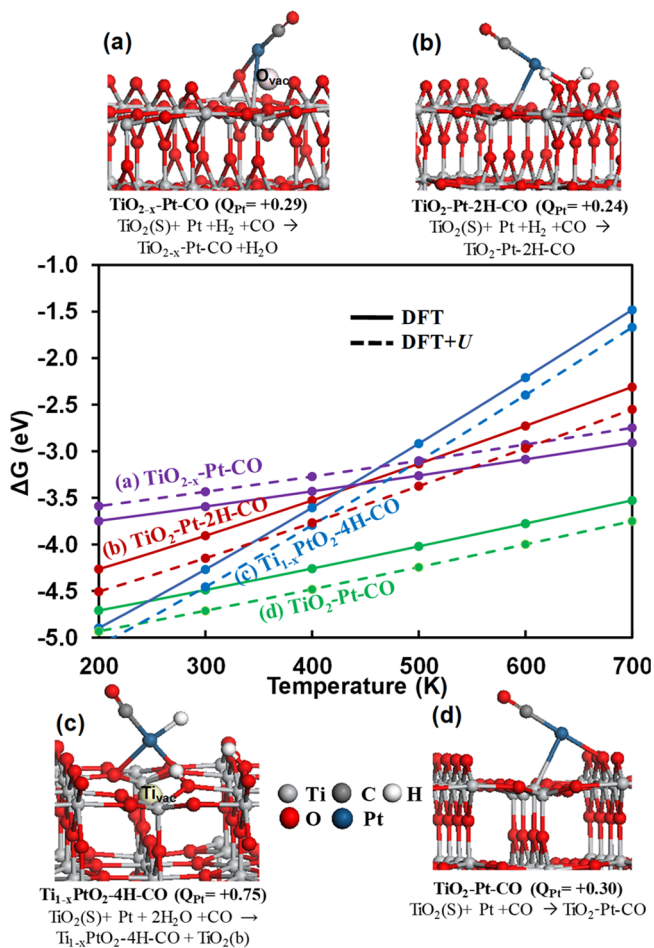


Figure 7. Gibbs free energies (ΔG) for the interaction of a Pt atom on a $\text{TiO}_2(110)$ surface under WGS reaction conditions. Side view of the optimized structures, together with the reactions used to calculate Gibbs free energies, are provided in the inset. $\text{TiO}_2(s)$ and $\text{TiO}_2(b)$ are the clean $\text{TiO}_2(110)$ surface and a TiO_2 bulk unit, respectively. Q_{Pt} is the Bader charge on the Pt atom. Reaction conditions of $P_{\text{CO}} = 0.1$, $P_{\text{H}_2\text{O}} = 0.2$, and $P_{\text{H}_2} = 0.4$ atm were used to calculate ΔG . [Adapted with permission from ref 137. Copyright 2016, American Chemical Society, Washington, DC.]

exhibit reasonably good activity for the WGS; however, the TOFs predicted for the doped surface are an order of

magnitude higher than those of the nondoped models. For both models, the CO_2 desorption process, which creates an oxygen vacancy, was identified as the rate-controlling process. Comparison of the kinetic results obtained for the single Pt sites with the earlier work on the $\text{Pt}_8/\text{TiO}_2(110)$ interface model under a specific experimental condition (Table 2) revealed many interesting phenomena. The redox pathway seems to operate on various types of Pt active sites supported on $\text{TiO}_2(110)$. The TOFs indicate that the edge interface Pt and the single-site Pt^{2+} sites are active for WGS at temperatures of <573 K, whereas the corner interface Pt sites are active at higher temperatures. It was further identified that the CO adsorption strength on Pt and the TiO_2 surface oxygen vacancy formation are the two main factors that determine the activity of these sites. The site with exergonic CO adsorption at low temperature (corner interface Pt) exhibits a high activation barrier and the site with exergonic oxygen vacancy formation (edge interface Pt) can reproduce experimentally observed reaction orders and rate-controlling processes. Since the redox pathway that operates on both the single Pt^{2+} sites and the Pt cluster sites depends on the oxygen vacancy formation on the TiO_2 surface, these models predict similar TOFs at low temperatures (<573 K). However, the contribution from the corner Pt sites should also be included to the overall activity of the Pt clusters and thus, the Pt clusters/nanoparticles could exhibit a higher activity at temperatures of >573 K, compared to the Pt^{2+} -doped TiO_2 surface. Overall, these results suggest that the single Pt^{2+} sites, if stabilized on a $\text{TiO}_2(110)$ surface, can be as active for the WGS as the Pt nanoclusters, which agrees with the experimental reports by Flytzani-Stephanopoulos and co-workers.¹⁴¹ Since one CO molecule remains strongly attached to the Pt^{2+} site throughout the catalytic cycle, this model could also explain the nondisappearance of the single-Pt-atom-related CO IR peak observed by Ding et al.,⁷⁵ which led them to conclude that the atomically dispersed Pt on titania supports are not active for the WGS. Here, the adoption of the same computational setup for various Pt sites allowed us to compare the activity of different Pt sites, identify the limiting factors for these catalysts, and understand different experimental observations.

2.4. Alkali-Stabilized Single Pt^{2+} Models. In accordance with various experimental studies, the computational studies discussed above indicated that the Pt^{2+} sites stabilized on

Table 2. Turnover Frequency (TOF), Apparent Activation Energy (E^{app}), Adsorption Energy of Reacting CO ($E_{\text{CO}}^{\text{ads}}$), Oxygen Vacancy Formation Energy (E^{vf})^a, and Reaction Orders Calculated from Microkinetic Reactor Analysis of the WGS Reaction for Different Active Site Models of Pt Supported on a $\text{TiO}_2(110)$ Surface^b

catalyst model	TOF (s^{-1})			E^{app} (eV)	$E_{\text{CO}}^{\text{ads}}$ (eV)	E^{vf} (eV)	rate-limiting step	Reaction Orders ($T = 573$ K)			
	at 473 K	at 573 K	at 673 K					CO	CO_2	H_2O	H_2
$\text{TiO}_2\text{-Pt}_8\text{-2CO}$ (edge interface Pt) ^c	2.0×10^{-1}	2.4×10^1	4.7×10^1	0.57	-0.79	-0.47	O-H bond dissociation	0.62	0.00	0.61	-0.19
$\text{TiO}_2\text{-Pt}_8\text{-2CO}$ (corner interface Pt) ^d	7.8×10^{-3}	1.0×10^1	1.1×10^3	1.63	-1.47	0.31	CO_2 desorption	0.01	0.00	0.01	0.00
$\text{Ti}_{1-x}\text{O}_2\text{-Pt-CO-4H}$ (Pt^{2+}) ^e	4.5×10^{-1}	8.6×10^0	5.1×10^1	0.66	-0.27	0.35	CO_2 desorption	1.00	0.00	0.04	0.00
$\text{TiO}_2\text{-Pt-CO}$ ($\text{Pt}^{\delta+}$) ^f experiment ^g	8.2×10^{-2}	5.9×10^{-1}	2.4×10^0	0.46	-0.59	0.50	CO_2 desorption	1.00	0.00	0.00	0.00
			6.0×10^{-1}	0.61				0.30	0.00	0.85	-0.67

^aOxygen vacancy formation energy calculated with reference to the reaction, $\text{Pt}/\text{TiO}_2 + \text{CO} \rightarrow \text{Pt}/\text{TiO}_{2-x} + \text{CO}_2$. ^b $P_{\text{CO}} = 0.1$, $P_{\text{H}_2\text{O}} = 0.2$, $P_{\text{CO}_2} = 0.1$, $P_{\text{H}_2} = 0.4$ atm. ^cSee ref 55. Results presented here slightly differ from the values reported in ref 55, since, here, we used the same adsorption area per site (S_{unit}) for all our models. ^dSee ref 103. ^eSee ref 137. ^fSee ref 136. ^gSee ref 93.

reducible oxides are active for the WGS. However, fabrication of isolated Pt atom sites on supports other than ceria had always been a challenging task, because of the high mobility of the metal atoms, which can agglomerate to form nanoparticles and only few studies reported successful synthesis of Pt atom catalysts on different supports.^{24,75,118,144,145} A series of studies reported by Flytzani-Stephanopoulos and co-workers suggested that addition of alkali ions can stabilize these single Pt²⁺ sites on various supports, and, at the same time, these alkali cations can also provide additional OH groups near the active site.^{24,140,141,143} According to their recent reports,^{24,141} alkali-stabilized Pt²⁺ ions stabilized on various supports, such as titania, silica, alumina, zeolites, and carbon, are all active for the WGS and these catalysts exhibit similar apparent activation barriers. They proposed that a common active site, described as Pt(II)-alkali-O_x(OH)_y, is responsible for the WGS activity in these catalysts and the support effect is indirect. They further demonstrated that an abundance of Pt nanoparticles was formed on all these supports in the absence of alkali elements and these nanoparticles exhibit a lower WGS activity than their single Pt²⁺ counterparts stabilized by alkali ions. The promotional effect of alkali addition was also observed for Pt nanoparticles on other supports.^{70,71,73,146–151} Earlier studies on alkali-doped Pt/CeO₂ catalysts by Davis and co-workers^{146,147} suggested that (i) the alkali dopants are located on both the platinum and ceria components and (ii) they electronically modify both the support and Pt species. The promotional effect of alkali on the Pt/TiO₂ catalyst was attributed to the alkali-induced reduction of Ti⁴⁺ surface species by creating oxygen vacancy sites at the Pt/TiO₂ interface sites.¹⁴⁸ Ribeiro and co-workers reported that the alkali promotion on the Pt/Al₂O₃ and Pt/TiO₂ catalysts is caused by the modification of the properties of the support alone⁷⁰ and, in the case of Pt/t-ZrO₂ catalysts,⁷¹ the Na ions stabilize the ZrO₂ in the tetragonal phase, which promotes the WGS reaction. Whereas, recent studies on alkali-promoted Pt/Al₂O₃ catalysts suggested that the alkali ions modify the electronic structure of Pt and, in turn, change the adsorption properties of platinum.^{149,150} Thus, more-targeted research efforts seem to be necessary to understand the exact role of alkali ions on the supported Pt nanoparticles. In the case of alkali-stabilized single-site Pt catalysts, similar questions remain with regard to specifying the exact role of the alkali ions. Do the alkali ions provide only stability for the Pt ions or do they actively participate in the mechanism? What is the mechanism of the WGS on these catalysts? In order to partially answer these questions, we performed new DFT calculations; first to identify an appropriate model for a Na-stabilized single-site Pt catalyst supported on TiO₂(110) and then to examine the WGS mechanism on that model. We used a similar computational setup and strategy as in our previous work on Pt²⁺-doped TiO₂, such that the activities of the single Pt²⁺ sites can be compared in the presence and absence of alkali ions and the role of alkali elements can be identified. A complete description of the computational setup and results from constrained thermodynamic analysis are provided in the Supporting Information. We initially performed all the calculations with the PBE functional, such that the kinetic results can be compared with those from our earlier work. Because of the presence of highly ionic Na cations in the current catalytic system, we additionally performed calculations with the nonempirical “strongly constrained and appropriately normed” (SCAN)¹⁵² meta-GGA functional, which is expected

to provide accurate structures and energies of diversely bonded materials.

The experimental studies by the Flytzani-Stephanopoulos group¹⁴¹ established that the use of NaOH, instead of NaNO₃, as a sodium precursor, with a Na:Pt atomic ratio of 10:1, resulted in the formation of stable single Pt(II)-O(OH)_x sites on various supports. Using this experimental setup as a basis for our model building, we first examined the interaction of 12 NaOH units on the TiO₂(110) surface and later replaced two of the Na atoms by a Pt atom to achieve the experimentally observed Na:Pt ratio. The number of O, H, and OH groups was optimized for each structure using the PBE functional. Our thermodynamic analysis, as described in the Supporting Information (Figure S1), revealed that the formation of single-layer structures in which all the Na atoms are in contact with the TiO₂ surface oxygens is highly favorable relative to double-layer structures of NaOH both in the presence and absence of Pt. Figures 8a and 8b illustrate the most stable

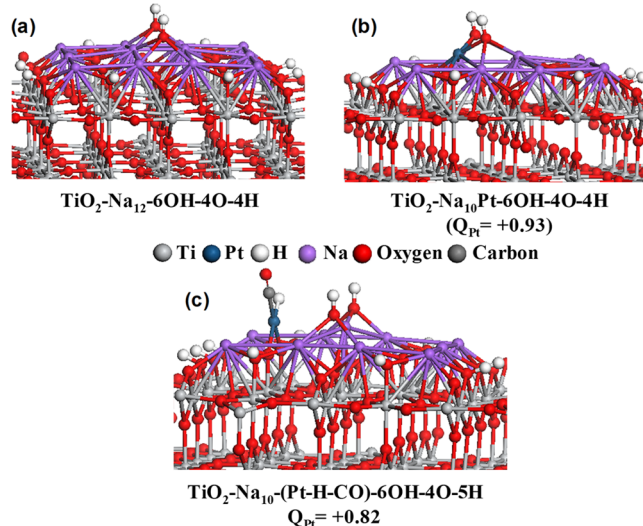


Figure 8. Stable structures identified from constrained ab initio thermodynamic analysis for the interaction of NaOH on TiO₂(110) in the (a) absence and (b) presence of Pt. (c) Stable structure identified for the Na-stabilized Pt site under WGS reaction conditions. Q_{Pt} is the Bader charge on the Pt atom.

structures identified from this analysis. Next, we performed a constrained thermodynamic analysis to examine the stability of this Na-stabilized single Pt site under experimental WGS reaction conditions ($P_{CO} = 0.11$, $P_{H_2O} = 0.26$, and $P_{H_2} = 0.26$ atm).¹⁴¹ Gibbs free energies calculated with PBE and SCAN functionals (Figure S2 in the Supporting Information) predicted that a square planar Pt²⁺ structure ($TiO_2-Na_{10}-(Pt-H-CO)-6OH-4O-5H$; see Figure 8c) in which the Pt is coordinated to two oxygen atoms, one CO, and one H is the stable structure at <700 K under WGS conditions. The Bader charge on Pt (+0.82) in this structure is very similar to the reported Bader charge on Pt in bulk PtO (+0.80).¹⁴⁰ Since this structure also provides two OH groups adsorbed on Na that are adjacent to the active Pt site, we refer to this catalyst model as $(H-CO)_{Pt}(OH-OH)_{Na}$ (IM1) and examined the WGS mechanism on this model, considering the formation of formate and carboxyl intermediates.

The intermediate and transition state (TS) structures involved in the WGS mechanism were first optimized using

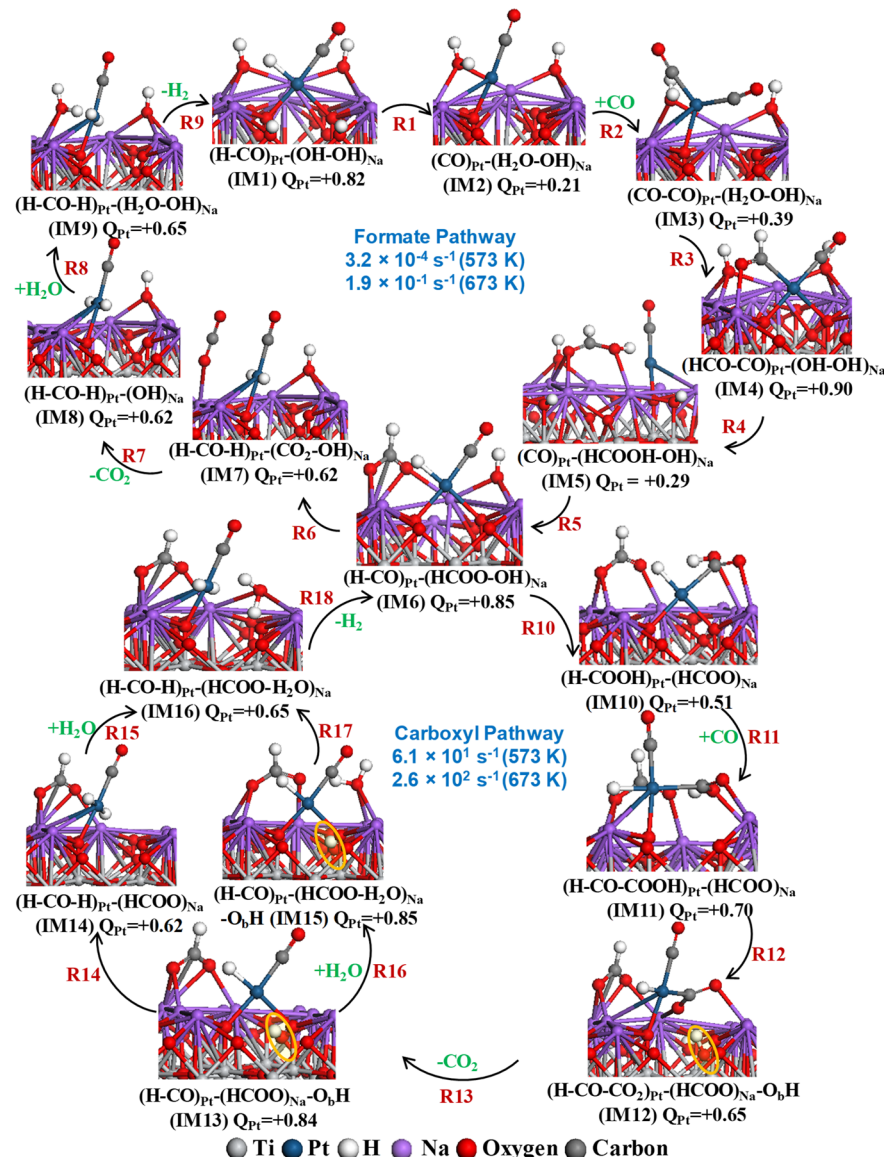


Figure 9. Formate and carboxyl pathways of the WGS reaction on the Na-stabilized single Pt^{2+} site supported on a $\text{TiO}_2(110)$ surface. The numbers provided for each pathway are the overall rates (in s^{-1}) calculated at two representative temperatures using the PBE functional ($P_{\text{CO}} = 0.1$ atm, $P_{\text{H}_2\text{O}} = 0.2$ atm, $P_{\text{CO}_2} = 0.1$ atm, $P_{\text{H}_2} = 0.4$ atm).

the PBE functional, and single-point energies were calculated on the PBE optimized structures using the meta-GGA SCAN functional. Our calculations suggested that the formation of formate intermediates are highly favorable on the Na sites and thus, we first examined the formate pathway. The minimum energy pathway identified for this mechanism involves nine elementary reactions and is illustrated in Figure 9. The TS structures are provided in the Supporting Information. Since direct CO adsorption on the square planar Pt^{2+} site (IM1) was found to be not favorable, the reaction proceeds via the spillover of H from Pt to OH (R1), forming a nearly neutral Pt and a H_2O adsorbed on Na (IM2). A second CO molecule then adsorbs (R2) on Pt ($E_{\text{ZPE}}^{\text{ads}} = -0.23$ eV, IM3) which reacts with H_2O (R3) forming a square planar Pt^{2+} with adsorbed HCO and CO species (IM4). In the following step (R4), the HCO species adsorbed on Pt reacts with OH adsorbed on neighboring Na forming a HCOOH intermediate (IM5) and the dissociation of HCOOH (R5) leads to the formation of a stable HCOO species adsorbed on Na and a square planar Pt^{2+}

site (IM6). Different possibilities of HCOO dissociation (R6) were explored and the lowest energy pathway identified ($E_{\text{ZPE}}^{\text{act}} = 1.44$ eV calculated with PBE) involves the transfer of H from HCOO to Pt with a linear CO_2 molecule adsorbed on Na (IM7). CO_2 easily desorbs (R7) from IM7, forming IM8, whereas direct H_2 formation from IM8 was found to have an activation barrier of nearly 2 eV. Thus, a H_2O -assisted H_2 formation was considered in the following steps (R8 and R9), which completes the catalytic cycle. The free-energy diagrams depicted in Figure 10 and Figure S4 in the Supporting Information indicate that the intermediate with HCOO species (IM6) is the stable species in this catalytic cycle and that the TS corresponding to the formation of H_2 (TS9) has the highest activation free energy. A microkinetic analysis of this pathway based on energies obtained with PBE functional and performed in the temperature range of 473–673 K under similar reaction conditions to those used in our earlier works^{55,103,136,137} ($P_{\text{CO}} = 0.1$, $P_{\text{CO}_2} = 0.1$, $P_{\text{H}_2\text{O}} = 0.2$, and P_{H_2}

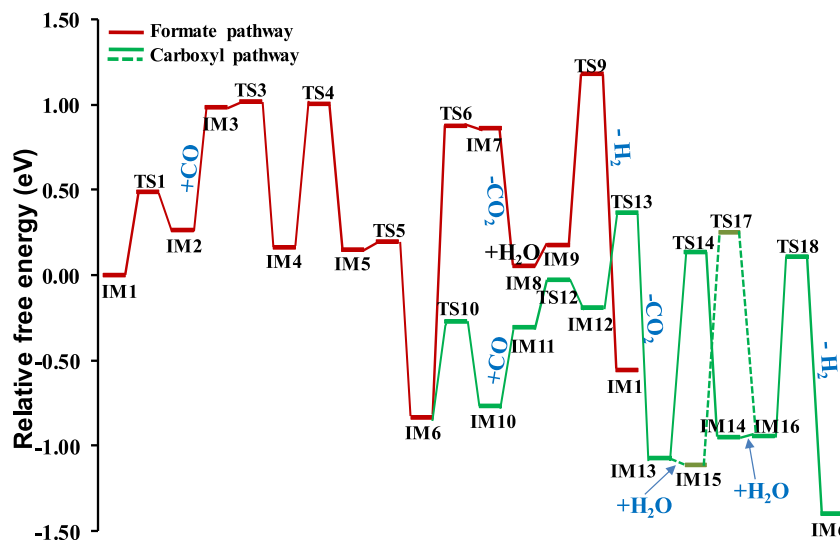


Figure 10. Free-energy profile for the formate and carboxyl pathways of the WGS reaction on the $\text{TiO}_2\text{-Na}_{10}\text{-}(\text{Pt}-\text{H}-\text{CO})\text{-6OH-4O-5H}$ model ($T = 500 \text{ K}$; $P_j(\text{gas}) = 1 \text{ atm}$) calculated with the SCAN functional on the structures optimized using the PBE functional. All energies are with reference to the sum of the energies of the initial state (IM1) and the reactant gas molecules.

Table 3. Turnover Frequency (TOF), Apparent Activation Energy (E^{app}), and Reaction Orders Calculated from Microkinetic Reactor Analysis of the WGS Reaction Mechanism on Na-Stabilized Single Pt^{2+} Sites Supported on a $\text{TiO}_2(110)$ Surface^a

method	TOF (s^{-1})			E^{app} (eV)	rate-limiting step	Reaction Orders ($T = 573 \text{ K}$)			
	473 K	573 K	673 K			CO	CO_2	H_2O	H_2
PBE//PBE	2.0×10^0	6.1×10^1	2.6×10^2	0.64	(R18) H_2 formation	0.13	0.00	0.91	0.00
SCAN//PBE	2.2×10^{-1}	2.1×10^1	1.0×10^2	0.77	(R13) CO_2 desorption	0.97	-0.01	0.06	0.00

^a $P_{\text{CO}} = 0.1$, $P_{\text{H}_2\text{O}} = 0.2$, $P_{\text{CO}_2} = 0.1$, $P_{\text{H}_2} = 0.4 \text{ atm}$.

= 0.4 atm) predicted a TOF of $1.3 \times 10^{-2} \text{ s}^{-1}$ (573 K) and an apparent activation barrier of 1.89 eV. The activation barriers calculated using the SCAN functional for elementary steps R6 and R9 are higher than those predicted by PBE (see Table S1 in the Supporting Information) and hence, this functional predicted a much lower TOF ($4.3 \times 10^{-5} \text{ s}^{-1}$ at 573 K) and a higher apparent activation barrier (2.17 eV) than PBE. The activation barriers predicted by both functionals for this formate pathway are much higher than the experimental value ($0.73 \pm 0.1 \text{ eV}$).¹⁴¹ Furthermore, a surface coverage of ~ 1 was observed for the HCOO intermediate (IM6) throughout the temperature range considered here, suggesting that the dissociation of HCOO species is not favorable under these conditions. Thus, in the following steps (R10–R18), we examined a carboxyl pathway in the presence of HCOO species.

The intermediate structures involved in the carboxyl pathway are illustrated in Figure 9, and the corresponding TS structures are provided in the Supporting Information. In the first step of the carboxyl pathway (R10), CO adsorbed on Pt and reacts with the OH adsorbed on Na, leading to the formation of a $-\text{COOH}$ intermediate (IM10). Then, a second CO adsorbs on Pt ($E_{\text{ZPE}}^{\text{ads}} = -0.55 \text{ eV}$ (PBE), R11) which leads to a breaking of one of the Pt–O bonds with the support (IM11). Dissociation of COOH occurs in the following step (R12) by transferring the H atom to the TiO_2 surface oxygen (IM12). Although the carboxyl species in IM11 is stabilized by H-bonding interaction with the HCOO species, dissociation of COOH by transferring the H atom to the formate species was found to be not favorable and optimization of different product structures considered for such dissociation converged back to

the reactant structure (IM11). Desorption of CO_2 from IM12 (R13) leads to the formation of the $(\text{H}-\text{CO})_{\text{pt}}$ species (IM13) with a H adsorbed on the surface bridging oxygen atom (O_b). Direct H-transfer from O_b to Pt followed by H_2O adsorption on the empty Na sites were considered in steps R14–R15. Alternatively, adsorption of H_2O on IM13 and transfer of H from H_2O to Pt were examined in steps R16 and R17. Here, we note that the reaction R17 includes two elementary steps, namely, transfer of H from H_2O to Pt and transfer of H from O_b to the OH adsorbed on Na. Our calculations suggested that once the H from H_2O in IM14 is transferred to Pt, the transfer of H from O_b to OH occurs without any barrier and, hence, we considered this process (R17) as a concerted H-transfer. The final step of this catalytic cycle (R18) is the formation of H_2 from IM16. The free-energy diagram calculated at a temperature of 500 K (Figure 10) suggests that the overall activation barrier for the carboxyl pathway is much lower than the formate pathway and that both CO_2 desorption (R13) and H_2 formation (R18) processes could affect the overall rate of the carboxyl pathway. In addition, the free energies calculated with both SCAN (Figure 10) and PBE (Figure S5 in the Supporting Information) indicate that the direct H-transfer from O_b to Pt (R14) could be preferred over the H_2O -assisted H-transfer (R17). Here, note that our attempts to include the $-\text{OH}$ species that are adsorbed on surface Ti atoms or the bridging oxygens of the TiO_2 surface in the reaction mechanism resulted in activation barriers of $>1.5 \text{ eV}$; therefore, these pathways are not expected to contribute to the overall rate.

The intermediate structures illustrated in Figure 9 indicate that the square planar structure of Pt is maintained throughout the carboxyl pathway, although the Bader charge on Pt is

slightly lower than that of Pt^{2+} (~ 0.8) for some of the intermediates. On the other hand, the structure of Pt changes from square planar to linear throughout the formate pathway and a reduction of Pt^{2+} to nearly neutral Pt was observed in this pathway. The zero-point energy (ZPE)-corrected reaction energies and activation barriers, forward rate constants, and equilibrium constants calculated at two different temperatures (573 and 673 K), using the PBE and SCAN functionals for the formate and carboxyl pathways, are summarized in **Tables S1 and S2** in the Supporting Information. These data are used to build a DFT-based microkinetic model including all 18 elementary reactions. The results obtained from microkinetic reactor analysis are presented in **Table 3**. The reaction rates presented in the inset of **Figure 9** reveal that the formate pathway exhibits 3–5 orders of magnitude lower rates than the carboxyl pathway at temperatures above 573 K and a much larger difference was observed between these two pathways at temperatures below 573 K. Clearly, the carboxyl pathway is the preferred mechanism for the WGS on Na-stabilized Pt^{2+} sites.

The apparent activation barriers predicted by both PBE (0.64 eV) and SCAN (0.77 eV) functionals are very close to the experimental value of Na-stabilized single-site Pt catalysts on various supports (0.73 ± 0.1 eV).¹⁴¹ Comparison of TOFs calculated with PBE functional with different Pt active site models (**Table 2**) revealed that the TiO_2 supported Na-stabilized Pt^{2+} sites do exhibit greater activity than the Pt clusters and single Pt sites stabilized on $\text{TiO}_2(110)$ —except for corner Pt interface sites that exhibit a slightly greater activity at 673 K. This result again agrees with the experimental observation by the Flytzani-Stephanopoulos group,¹⁴¹ that the Na-free Pt catalysts on various supports (including TiO_2) form an abundance of Pt nanoparticles and exhibit a relatively lower WGS activity than their Na-containing counterparts with single-atom-centric Pt sites. Although the TOFs and apparent activation barriers calculated with the SCAN functional are not very different from those computed with the PBE functional, significant differences are observed in the reaction orders and rate-limiting steps. While the PBE functional predicted that the intermediate, $(\text{H}-\text{CO})_{\text{Pt}}-(\text{HCOO})_{\text{Na}}-\text{O}_\text{b}\text{H}$ (IM13) is the dominant species with a surface coverage (θ) of 0.9 between 573 K and 673 K, the SCAN functional predicted that the intermediate, $(\text{H}-\text{CO})_{\text{Pt}}-(\text{HCOO}-\text{OH})_{\text{Na}}$ (IM6) is the dominant species ($\theta = 0.8$) in this temperature range (see **Table S3** and **Figure S6** in the Supporting Information). Accordingly, the rate-controlling step and reaction orders change between these two functionals. Throughout this work (i.e., during our thermodynamic analysis and mechanistic study), we noticed that the PBE functional predicted lower energies for structures when H atoms are added to the TiO_2 surface oxygens (reducing the surface), compared to the SCAN functional. This is probably due to the commonly known self-interaction error associated with standard DFT functionals that tend to delocalize electrons and holes in defective oxides. While the self-interaction error is not completely removed in the meta-GGA SCAN functional, this functional has been shown to predict accurate geometries and energies of diversely bonded molecules and materials that contain covalent, metallic, ionic, hydrogen and van der Waals bonds.¹⁵³ Thus, we expect that the kinetic results predicted by the SCAN functional could be appropriate in this case due to the presence of highly ionic Na cations.

Overall, this study revealed that Na-stabilized Pt^{2+} sites supported on TiO_2 can exhibit a high activity for the WGS.

Stable formate species can easily be formed on the Na sites adjacent to the active Pt site; however, these formate species only act as spectators. Whenever OH species are available next to the CO adsorbed on an active Pt site, the carboxyl pathway prevails, resulting in a higher TOF and lower apparent activation barrier. Since the effect of alkali addition on the Pt clusters is not investigated here, we can only conclude that the TiO_2 supported Na-stabilized Pt^{2+} sites are more active than the Pt^{2+} -doped TiO_2 surface and the WGS mechanisms differ in these two catalysts. The role of Na cations in these highly active catalysts can be multifold:

- (i) Na cations stabilize additional oxygen atoms on the TiO_2 support that provide anchoring sites for the Pt cation
- (ii) Na cations also stabilize additional OH species that actively participate in the mechanism.
- (iii) H_2O adsorption is highly favorable on the Na sites, compared to the Pt metal surfaces, which assists the formation of H_2 .

Hence, the WGS mechanism on Na-stabilized Pt^{2+} sites can be classified as bifunctional, similar to the reducible-oxide-supported Pt catalysts, in which the Pt cation adsorbs and activates CO and the Na cations provide reacting OH species and activate H_2O . The unique activity of these catalysts emerges from such cooperative interactions between the Pt^{2+} binding site, reacting molecules, and the surrounding Na cations.

3. IDENTIFYING ACTIVE SITES FOR THE WGS UNDER UNCERTAINTY

The computational results summarized in **section 2** reveal that first-principles-based microkinetic models are vital in understanding the observed macroscale reaction kinetics and the relative activity of different active sites. However, commonly used DFT methods based on the generalized gradient approximation have inadequacies due to exchange-correlation approximations, which can introduce significant errors in the prediction of TOFs, apparent activation barriers, and reaction orders. At a temperature of 500 K, an error of <0.1 eV is required for an accuracy of 1 order of magnitude of an elementary rate and equilibrium constant. In the case of Pt catalysts supported on TiO_2 and CeO_2 , the computational studies summarized in the above section predicted that the adsorption strength of CO on Pt and the stability of the oxygen vacancy structure are two important factors that determine the overall activity of these catalysts. Can the DFT methods used here accurately predict these two determining factors? The PBE functional used in these works is known to underestimate the gas-phase energy of the CO molecule and, in turn, overestimates the WGS reaction free energy by ~ 0.4 eV. A statistical analysis of a set of gas-phase reactions, including CO, CO_2 , H_2 , and H_2O , performed by Peterson et al.¹⁵⁴ and by us,¹⁰³ suggested that this error arises mainly from the energy of the CO molecule predicted by the PBE functional. However, how much of this error in gas-phase energy is transferred to an adsorbed CO molecule or transition state is currently unknown. In the case of oxygen vacancy structures, the standard DFT methods fail to produce correct electronic structures, because of the well-known problem of the self-interaction error. Although the use of the DFT+U approach can circumvent this problem somewhat and is affordable for larger systems, identifying an appropriate “U” parameter for a

specific element that is transferrable across different atomic environments is still problematic. Moreover, the ability of this approach to correctly describe the strength of chemical bonds in addition to correct electronic structures is also unknown. A proposed solution to these problems is to quantify uncertainties in these DFT calculations using Bayesian statistical tools, propagate them to the macroscopic quantities of interest, such as TOF, apparent activation barrier, reaction orders, etc., and guide the process of drawing conclusions under uncertainty.^{6,16,17,155}

Medford et al.¹⁵⁵ introduced a general method for estimating the uncertainty in calculated DFT energies by choosing an ensemble of exchange-correlation functionals for a set of adsorption energies which are then used to calculate the rates of the ammonia synthesis via microkinetic modeling. It was found that (i) the uncertainties on the calculated rates are strongly dependent on the reaction conditions and catalyst material, and (ii) trends in catalytic activity are better described than absolute rates. In another work, Sutton et al.⁶ proposed a correlative global sensitivity analysis and uncertainty quantification to assess the predictive ability of complex kinetic models parametrized using DFT calculations and applied this methodology to ethanol steam reforming on a Pt/Al₂O₃ catalyst. They showed that correlation in DFT-calculated parameters significantly alter the influential parameters and their method can, in conjunction with experimental data, provide valuable information on the catalyst active site and identify influential missing reaction pathways. An uncertainty quantification (UQ) framework has recently been applied to the WGS mechanism investigated on the Pt₈/TiO₂(110) catalyst model discussed above, where information obtained from three different classes of functionals, GGA (PBE and RPBE), meta-GGA (M06L), and hybrid (HSE) functionals, were used to generate a probabilistic model for the free energies of every state in the catalyst system.¹⁶ It was found that the active site model used in this study captures various experimental kinetic data; however, the probability densities for the TOFs, reaction orders, and apparent activation barriers were relatively wide due to different DFT functionals predicting different activation barriers and oxygen vacancy formation energies. Using Kullback–Leibler divergence, it was however still possible to conclude that the CO-promoted redox pathway, which was originally identified as a dominant pathway when using the PBE functional, is also the dominant pathway for the WGS on the Pt/TiO₂ catalysts under uncertainty. In another study,¹⁷ this UQ framework has been extended and applied to three different active site models—a Pt(111) terrace model and the edge and corner interface sites of the Pt₈/TiO₂(110) model—to identify the most active site in the experimental catalysts. By rigorously combining the DFT based models with experimental data, significant evidence was found against the Pt terrace sites, compared to the interface edge and corner sites, suggesting that the Pt terrace sites are not active for the WGS and the support plays an active role in the mechanism in the experimental catalysts included in this study.^{63,70,93} Posterior predictive checks used to discriminate between the edge and corner sites furthermore suggested that the edge interface sites are the active sites for WGS in the experimental catalysts. The approach was further used to predict the rate-controlling steps while considering the uncertainties under different reaction conditions. Under all conditions, surface O–H and water dissociation processes were found to be key rate-controlling steps. Since the

developed UQ framework used in this work is not limited to the application of the WGS, the use of this methodology is advocated to other catalytic processes where identification of the active site is of critical importance.

4. CONCLUSIONS

In this Perspective, we have analyzed recent developments in the computational study of the WGS mechanism on supported Pt catalysts considering various active site models, such as unsupported Pt surface models, Pt clusters supported on reducible oxides, and supported single Pt sites in the presence and absence of alkali ions. The focus of this Perspective is not just to understand the mechanism of the WGS on these catalysts or to determine which site is more active for the WGS, but to understand how, generally, computational studies are helpful in attaining atomic level information and understanding experimental observations. In that context, a critical analysis is made on the accuracy of two important parameters, model and method, which form the basis for any computational catalysis study. Selecting an appropriate active site model is the first critical step in any computational catalysis study. Only if a characteristic active site model has been selected can reasonable results be obtained that are comparable with experimental observations. Here, it has been shown that computations performed on unsupported Pt surface models could not reproduce experimentally observed reaction orders and activation barriers of Pt catalysts supported on both active and inert supports. For reducible-oxide-supported Pt catalysts, a multistep strategy is necessary to correlate computational results with experimental observations and identify limiting factors. Careful consideration of the chemical environment of the catalyst system and identification of the local environment of the active site under reaction conditions through thermodynamic analysis are imperative in building a catalyst model for a mechanistic study. The computational results summarized in section 2 for the WGS mechanism over various Pt active site models show strong evidence that DFT calculations, together with kinetic analysis performed on reasonable active site models, can provide significant insights into the active sites, reaction mechanisms, and specific function of various multiphase sites for the WGS. It was also possible to identify the promoting/limiting factors for the high/low WGS activity of different catalysts and explain the role of support oxide, metal, and alkali cations. It is interesting to note that the alkali cations behave similar to the reducible oxide supports by supplying OH species for the WGS reaction and activating H₂O molecules. Such an understanding of the specific role of alkali cations in the Na-stabilized Pt²⁺ catalysts for the WGS can open up new possibilities in the design of alkali-stabilized single atom catalysts that are inexpensive and, at the same time, highly active and selective toward various heterogeneous catalytic processes.

The method accuracy is another cornerstone of computational chemistry and compromises often must be made between the model and method accuracy while handling large catalyst models. As discussed above, DFT calculations have become indispensable in providing an atomistic framework for understanding reaction mechanisms and have been applied successfully in predicting experimentally observed trends. However, because of inadequacies that arise from the exchange-correlation approximations of the DFT functionals, the accuracy of calculated energy differences is only between 0.2 eV to 0.4 eV and there is no guarantee that “error

cancellation" reduces this error significantly. In such cases, complementing the DFT studies of reaction mechanisms with a systematic Bayesian uncertainty quantification study that correlates theoretical predictions with experimental observations in the presence of the uncertainties in DFT methods has been found to be very helpful in the identification of meaningful active site models and practical descriptors for the discovery of novel catalysts.

■ ASSOCIATED CONTENT

Supporting Information

The Supporting Information is available free of charge on the ACS Publications website at DOI: [10.1021/acscatal.9b01560](https://doi.org/10.1021/acscatal.9b01560).

Computational details for the new calculations performed on the Na-stabilized single Pt sites; ab initio thermodynamic analysis performed to identify a catalyst model for the Na-stabilized single Pt sites (Figures S1 and S2); details of the microkinetic model used with the structure highlighting the atoms displaced for vibrational frequency calculations (Figure S3); energy profiles calculated for the formate (Figure S4) and carboxyl (Figures S5 and S6) pathways; transition states involved in the formate and carboxyl pathways (Figures S7 and S8); reaction energies and activation barriers for the 18 elementary steps (Table S1); forward rate constants and equilibrium constants calculated at different temperatures (Table S2); and surface coverages of various intermediates calculated at different temperatures (Table S3) ([PDF](#))

■ AUTHOR INFORMATION

Corresponding Author

*E-mail: heyden@cec.sc.edu.

ORCID

Andreas Heyden: [0000-0002-4939-7489](https://orcid.org/0000-0002-4939-7489)

Notes

The authors declare no competing financial interest.

■ ACKNOWLEDGMENTS

This work was supported by the National Science Foundation, under Grant No. CBET-1254352, and in part by XSEDE resources provided by the San Diego Supercomputer Center (SDSC) and Texas Advanced Computing Center (TACC), under Grant No. TG-CTS090100. Furthermore, a portion of this research was performed at the U.S. Department of Energy facilities located at the National Energy Research Scientific Computing Center (NERSC), under Contract No. DE-AC02-05CH11231 and Pacific Northwest National Laboratory (Ringgold ID 130367, Grant Proposal Nos. 49246 and 50576). Finally, computing resources from High-Performance Computing clusters located at University of South Carolina are gratefully acknowledged.

■ REFERENCES

- (1) Friend, C. M.; Xu, B. J. Heterogeneous Catalysis: A Central Science for a Sustainable Future. *Acc. Chem. Res.* **2017**, *50*, 517–521.
- (2) Spivey, J. J.; Krishna, K. S.; Kumar, C. S. S. R.; Dooley, K. M.; Flake, J. C.; Haber, L. H.; Xu, Y.; Janik, M. J.; Sinnott, S. B.; Cheng, Y. T.; Liang, T.; Sholl, D. S.; Manz, T. A.; Diebold, U.; Parkinson, G. S.; Bruce, D. A.; de Jongh, P. Synthesis, Characterization, and Computation of Catalysts at the Center for Atomic-Level Catalyst Design. *J. Phys. Chem. C* **2014**, *118*, 20043–20069.

(3) Van Speybroeck, V.; Hemelsoet, K.; Joos, L.; Waroquier, M.; Bell, R. G.; Catlow, C. R. A. Advances in Theory and their Application Within the Field of Zeolite Chemistry. *Chem. Soc. Rev.* **2015**, *44*, 7044–7111.

(4) Klippenstein, S. J.; Pande, V. S.; Truhlar, D. G. Chemical Kinetics and Mechanisms of Complex Systems: A Perspective on Recent Theoretical Advances. *J. Am. Chem. Soc.* **2014**, *136*, 528–546.

(5) Honkala, K.; Hellman, A.; Remediakis, I. N.; Logadottir, A.; Carlsson, A.; Dahl, S.; Christensen, C. H.; Norskov, J. K. Ammonia Synthesis from First-Principles Calculations. *Science* **2005**, *307*, 555–558.

(6) Sutton, J. E.; Guo, W.; Katsoulakis, M. A.; Vlachos, D. G. Effects of Correlated Parameters and Uncertainty in Electronic-Structure-Based Chemical Kinetic Modelling. *Nat. Chem.* **2016**, *8*, 331–337.

(7) Norskov, J. K.; Bligaard, T.; Rossmeisl, J.; Christensen, C. H. Towards the Computational Design of Solid Catalysts. *Nat. Chem.* **2009**, *1*, 37–46.

(8) Topsoe, H.; Hinnemann, B.; Norskov, J. K.; Lauritsen, J. V.; Besenbacher, F.; Hansen, P. L.; Hytoft, G.; Egeberg, R. G.; Knudsen, K. G. The Role of Reaction Pathways and Support Interactions in the Development of High Activity Hydrotreating Catalysts. *Catal. Today* **2005**, *107*–108, 12–22.

(9) Linic, S.; Jankowiak, J.; Bartea, M. A. Selectivity Driven Design of Bimetallic Ethylene Epoxidation Catalysts from First Principles. *J. Catal.* **2004**, *224*, 489–493.

(10) Falivene, L.; Kozlov, S. M.; Cavallo, L. Constructing Bridges between Computational Tools in Heterogeneous and Homogeneous Catalysis. *ACS Catal.* **2018**, *8*, 5637–5656.

(11) Pidko, E. A. Toward the Balance between the Reductionist and Systems Approaches in Computational Catalysis: Model versus Method Accuracy for the Description of Catalytic Systems. *ACS Catal.* **2017**, *7*, 4230–4234.

(12) Anisimov, V. I.; Zaanen, J.; Andersen, O. K. Band Theory and Mott Insulators - Hubbard-U Instead of Stoner-I. *Phys. Rev. B: Condens. Matter Mater. Phys.* **1991**, *44*, 943–954.

(13) Liechtenstein, A. I.; Anisimov, V. I.; Zaanen, J. Density-Functional Theory and Strong-Interactions - Orbital Ordering in Mott-Hubbard Insulators. *Phys. Rev. B: Condens. Matter Mater. Phys.* **1995**, *52*, R5467–R5470.

(14) Pacchioni, G. Modeling Doped and Defective Oxides in Catalysis with Density Functional Theory Methods: Room for Improvements. *J. Chem. Phys.* **2008**, *128*, 182505.

(15) Galagali, N.; Marzouk, Y. M. Bayesian Inference of Chemical Kinetic Models from Proposed Reactions. *Chem. Eng. Sci.* **2015**, *123*, 170–190.

(16) Walker, E.; Ammal, S. C.; Terejanu, G. A.; Heyden, A. Uncertainty Quantification Framework Applied to the Water-Gas Shift Reaction over Pt-Based Catalysts. *J. Phys. Chem. C* **2016**, *120*, 10328–10339.

(17) Walker, E. A.; Mitchell, D.; Terejanu, G. A.; Heyden, A. Identifying Active Sites of the Water-Gas Shift Reaction over Titania Supported Platinum Catalysts under Uncertainty. *ACS Catal.* **2018**, *8*, 3990–3998.

(18) Newsome, D. S. The Water-Gas Shift Reaction. *Catal. Rev.: Sci. Eng.* **1980**, *21*, 275–318.

(19) Ratnasamy, C.; Wagner, J. P. Water Gas Shift Catalysis. *Catal. Rev.: Sci. Eng.* **2009**, *51*, 325–440.

(20) Smith R J, B.; Loganathan, M.; Shantha, M. S. A Review of the Water Gas Shift Reaction Kinetics. *Int. J. Chem. React. Eng.* **2010**, *8*, Review R4 (DOI: [10.2202/1542-6580.2238](https://doi.org/10.2202/1542-6580.2238)).

(21) Huang, S. C.; Lin, C. H.; Wang, J. H. Trends of Water Gas Shift Reaction on Close-Packed Transition Metal Surfaces. *J. Phys. Chem. C* **2010**, *114*, 9826–9834.

(22) Lin, C. H.; Chen, C. L.; Wang, J. H. Mechanistic Studies of Water-Gas-Shift Reaction on Transition Metals. *J. Phys. Chem. C* **2011**, *115*, 18582–18588.

(23) Pal, D. B.; Chand, R.; Upadhyay, S. N.; Mishra, P. K. Performance of Water Gas Shift Reaction Catalysts: A Review. *Renewable Sustainable Energy Rev.* **2018**, *93*, 549–565.

- (24) Yang, M.; Flytzani-Stephanopoulos, M. Design of Single-Atom Metal Catalysts on Various Supports for the Low-Temperature Water-Gas Shift Reaction. *Catal. Today* **2017**, *298*, 216–225.
- (25) Liu, L. C.; Corma, A. Metal Catalysts for Heterogeneous Catalysis: From Single Atoms to Nanoclusters and Nanoparticles. *Chem. Rev.* **2018**, *118*, 4981–5079.
- (26) Sakurai, H.; Ueda, A.; Kobayashi, T.; Haruta, M. Low-Temperature Water-Gas Shift Reaction over Gold Deposited on TiO₂. *Chem. Commun.* **1997**, 271–272.
- (27) Burch, R. Gold Catalysts for Pure Hydrogen Production in the Water-Gas Shift Reaction: Activity, Structure and Reaction Mechanism. *Phys. Chem. Chem. Phys.* **2006**, *8*, 5483–5500.
- (28) Rodriguez, J. A.; Evans, J.; Graciani, J.; Park, J. B.; Liu, P.; Hrbek, J.; Sanz, J. F. High Water-Gas Shift Activity in TiO₂(110) Supported Cu and Au Nanoparticles: Role of the Oxide and Metal Particle Size. *J. Phys. Chem. C* **2009**, *113*, 7364–7370.
- (29) Rodriguez, J. A.; Liu, R.; Hrbek, J.; Perez, M.; Evans, J. Water-Gas Shift Activity of Au and Cu Nanoparticles Supported on Molybdenum Oxides. *J. Mol. Catal. A: Chem.* **2008**, *281*, 59–65.
- (30) Chen, Y.; Wang, H. F.; Burch, R.; Hardacre, C.; Hu, P. New Insight into Mechanisms in Water-Gas-Shift Reaction on Au/CeO₂(111): A Density Functional Theory and Kinetic Study. *Faraday Discuss.* **2011**, *152*, 121–133.
- (31) Sandoval, A.; Gomez-Cortes, A.; Zanella, R.; Diaz, G.; Saniger, J. M. Gold Nanoparticles: Support Effects for the WGS reaction. *J. Mol. Catal. A: Chem.* **2007**, *278*, 200–208.
- (32) Tabakova, T.; Idakiev, V.; Andreeva, D.; Mitov, I. Influence of the Microscopic Properties of the Support on the Catalytic Activity of Au/ZnO, Au/ZrO₂, Au/Fe₂O₃, Au/Fe₂O₃-ZnO, Au/Fe₂O₃-ZrO₂ Catalysts for the WGS reaction. *Appl. Catal., A* **2000**, *202*, 91–97.
- (33) Rodriguez, J. A.; Liu, P.; Hrbek, J.; Evans, J.; Perez, M. Water Gas Shift Reaction on Cu and Au Nanoparticles Supported on CeO₂(111) and ZnO(0001): Intrinsic Activity and Importance of Support Interactions. *Angew. Chem., Int. Ed.* **2007**, *46*, 1329–1332.
- (34) Fu, Q.; Saltsburg, H.; Flytzani-Stephanopoulos, M. Active Nonmetallic Au and Pt Species on Ceria-Based Water-Gas Shift Catalysts. *Science* **2003**, *301*, 935–938.
- (35) Gong, J. L. Structure and Surface Chemistry of Gold-Based Model Catalysts. *Chem. Rev.* **2012**, *112*, 2987–3054.
- (36) Williams, W. D.; Shekhar, M.; Lee, W. S.; Kispersky, V.; Delgass, W. N.; Ribeiro, F. H.; Kim, S. M.; Stach, E. A.; Miller, J. T.; Allard, L. F. Metallic Corner Atoms in Gold Clusters Supported on Rutile Are the Dominant Active Site during Water-Gas Shift Catalysis. *J. Am. Chem. Soc.* **2010**, *132*, 14018–14020.
- (37) Shekhar, M.; Wang, J.; Lee, W. S.; Williams, W. D.; Kim, S. M.; Stach, E. A.; Miller, J. T.; Delgass, W. N.; Ribeiro, F. H. Size and Support Effects for the Water-Gas Shift Catalysis over Gold Nanoparticles Supported on Model Al₂O₃ and TiO₂. *J. Am. Chem. Soc.* **2012**, *134*, 4700–4708.
- (38) Park, J. B.; Graciani, J.; Evans, J.; Stacchiola, D.; Senanayake, S. D.; Barrio, L.; Liu, P.; Sanz, J. F.; Hrbek, J.; Rodriguez, J. A. Gold, Copper, and Platinum Nanoparticles Dispersed on CeO_x/TiO₂(110) Surfaces: High Water-Gas Shift Activity and the Nature of the Mixed-Metal Oxide at the Nanometer Level. *J. Am. Chem. Soc.* **2010**, *132*, 356–363.
- (39) Ta, N.; Liu, J. Y.; Chenna, S.; Crozier, P. A.; Li, Y.; Chen, A. L.; Shen, W. J. Stabilized Gold Nanoparticles on Ceria Nanorods by Strong Interfacial Anchoring. *J. Am. Chem. Soc.* **2012**, *134*, 20585–20588.
- (40) Mudiyanselage, K.; Senanayake, S. D.; Feria, L.; Kundu, S.; Baber, A. E.; Graciani, J.; Vidal, A. B.; Agnoli, S.; Evans, J.; Chang, R.; Axnanda, S.; Liu, Z.; Sanz, J. F.; Liu, P.; Rodriguez, J. A.; Stacchiola, D. J. Importance of the Metal-Oxide Interface in Catalysis: In Situ Studies of the Water-Gas Shift Reaction by Ambient-Pressure X-ray Photoelectron Spectroscopy. *Angew. Chem., Int. Ed.* **2013**, *52*, 5101–5105.
- (41) Soria, M. A.; Perez, P.; Carabineiro, S. A. C.; Maldonado-Hodar, F. J.; Mendes, A.; Madeira, L. M. Effect of the Preparation Method on the Catalytic Activity and Stability of Au/Fe₂O₃ Catalysts in the Low-Temperature Water-Gas Shift Reaction. *Appl. Catal., A* **2014**, *470*, 45–55.
- (42) Chen, C. Q.; Ruan, C. X.; Zhan, Y. Y.; Lin, X. Y.; Zheng, Q.; Wei, K. M. The Significant Role of Oxygen Vacancy in Cu/ZrO₂ Catalyst for Enhancing Water-Gas-Shift Performance. *Int. J. Hydrogen Energy* **2014**, *39*, 317–324.
- (43) Zhao, Z. J.; Li, Z. L.; Cui, Y. R.; Zhu, H. Y.; Schneider, W. F.; Delgass, W. N.; Ribeiro, F.; Greeley, J. Importance of Metal-Oxide Interfaces in Heterogeneous catalysis: A Combined DFT, Microkinetic, and Experimental Study of Water-Gas Shift on Au/MgO. *J. Catal.* **2017**, *345*, 157–169.
- (44) Yao, S. Y.; Zhang, X.; Zhou, W.; Gao, R.; Xu, W. Q.; Ye, Y. F.; Lin, L. L.; Wen, X. D.; Liu, P.; Chen, B. B.; Crumlin, E.; Guo, J. H.; Zuo, Z. J.; Li, W. Z.; Xie, J. L.; Lu, L.; Kiely, C. J.; Gu, L.; Shi, C.; Rodriguez, J. A.; Ma, D. Atomic-Layered Au Clusters on Alpha-MoC as Catalysts for the Low-Temperature Water-Gas Shift Reaction. *Science* **2017**, *357*, 389–393.
- (45) Rodriguez, J. A.; Grinter, D. C.; Liu, Z. Y.; Palomino, R. M.; Senanayake, S. D. Ceria-Based Model Catalysts: Fundamental Studies on the Importance of the Metal-Ceria Interface in CO Oxidation, the Water-Gas Shift, CO₂ Hydrogenation, and Methane and Alcohol Reforming. *Chem. Soc. Rev.* **2017**, *46*, 1824–1841.
- (46) Chen, C. Q.; Zhan, Y. Y.; Zhou, J. K.; Li, D. L.; Zhang, Y. J.; Lin, X. Y.; Jiang, L. L.; Zheng, Q. Cu/CeO₂ Catalyst for Water-Gas Shift Reaction: Effect of CeO₂ Pretreatment. *ChemPhysChem* **2018**, *19*, 1448–1455.
- (47) Carter, J. H.; Hutchings, G. J. Recent Advances in the Gold-Catalysed Low-Temperature Water-Gas Shift Reaction. *Catalysts* **2018**, *8*, 627.
- (48) Fu, X.-P.; Guo, L.-W.; Wang, W.-W.; Ma, C.; Jia, C.-J.; Wu, K.; Si, R.; Sun, L.-D.; Yan, C.-H. Direct Identification of Active Surface Species for the Water-Gas Shift Reaction on a Gold-Ceria Catalyst. *J. Am. Chem. Soc.* **2019**, *141*, 4613–4623.
- (49) Thomas, J. M.; Midgley, P. A. The Merits of Static and Dynamic High-Resolution Electron Microscopy (HREM) for the Study of Solid Catalysts. *ChemCatChem* **2010**, *2*, 783–798.
- (50) Yang, J. C.; Small, M. W.; Grieshaber, R. V.; Nuzzo, R. G. Recent Developments and Applications of Electron Microscopy to Heterogeneous Catalysis. *Chem. Soc. Rev.* **2012**, *41*, 8179–8194.
- (51) Roldan Cuenya, B.; Behafarid, F. Nanocatalysis: Size- and Shape-Dependent Chemisorption and Catalytic Reactivity. *Surf. Sci. Rep.* **2015**, *70*, 135–187.
- (52) Salciccioli, M.; Stamatakis, M.; Caratzoulas, S.; Vlachos, D. G. A Review of Multiscale Modeling of Metal-Catalyzed Reactions: Mechanism Development for Complexity and Emergent Behavior. *Chem. Eng. Sci.* **2011**, *66*, 4319–4355.
- (53) Gupta, A.; Khammash, M. Unbiased Estimation of Parameter Sensitivities for Stochastic Chemical Reaction Networks. *Siam J. Sci. Comput.* **2013**, *35*, A2598–A2620.
- (54) Vlachos, D. G.; Mhadeshwar, A. B.; Kaisare, N. S. Hierarchical Multiscale Model-Based Design of Experiments, Catalysts, and Reactors for Fuel Processing. *Comput. Chem. Eng.* **2006**, *30*, 1712–1724.
- (55) Ammal, S. C.; Heyden, A. Origin of the Unique Activity of Pt/TiO₂ Catalysts for the Water-Gas Shift Reaction. *J. Catal.* **2013**, *306*, 78–90.
- (56) Grabow, L. C.; Gokhale, A. A.; Evans, S. T.; Dumesic, J. A.; Mavrikakis, M. Mechanism of the Water Gas Shift Reaction on Pt: First Principles, Experiments, and Microkinetic Modeling. *J. Phys. Chem. C* **2008**, *112*, 4608–4617.
- (57) Stamatakis, M.; Chen, Y.; Vlachos, D. G. First-Principles-Based Kinetic Monte Carlo Simulation of the Structure Sensitivity of the Water-Gas Shift Reaction on Platinum Surfaces. *J. Phys. Chem. C* **2011**, *115*, 24750–24762.
- (58) Flaherty, D. W.; Yu, W. Y.; Pozun, Z. D.; Henkelman, G.; Mullins, C. B. Mechanism for the Water-Gas Shift Reaction on Monofunctional Platinum and Cause of Catalyst Deactivation. *J. Catal.* **2011**, *282*, 278–288.

- (59) Carrasquillo-Flores, R.; Gallo, J. M. R.; Hahn, K.; Dumesic, J. A.; Mavrikakis, M. Density Functional Theory and Reaction Kinetics Studies of the Water-Gas Shift Reaction on Pt-Re Catalysts. *ChemCatChem* **2013**, *5*, 3690–3699.
- (60) Clay, J. P.; Greeley, J. P.; Ribeiro, F. H.; Delgass, W. N.; Schneider, W. F. DFT Comparison of Intrinsic WGS Kinetics over Pd and Pt. *J. Catal.* **2014**, *320*, 106–117.
- (61) Kalamaras, C. M.; Gonzalez, I. D.; Navarro, R. M.; Fierro, J. L. G.; Efsthathiou, A. M. Effects of Reaction Temperature and Support Composition on the Mechanism of Water-Gas Shift Reaction over Supported-Pt Catalysts. *J. Phys. Chem. C* **2011**, *115*, 11595–11610.
- (62) Hilaire, S.; Wang, X.; Luo, T.; Gorte, R. J.; Wagner, J. A Comparative Study of Water-Gas-Shift Reaction over Ceria Supported Metallic Catalysts. *Appl. Catal., A* **2001**, *215*, 271–278.
- (63) Kalamaras, C. M.; Panagiotopoulou, P.; Kondarides, D. I.; Efsthathiou, A. M. Kinetic and Mechanistic Studies of the Water-Gas Shift Reaction on Pt/TiO₂ Catalyst. *J. Catal.* **2009**, *264*, 117–129.
- (64) Azzam, K. G.; Babich, I. V.; Seshan, K.; Lefferts, L. Bifunctional Catalysts for Single-Stage Water-Gas Shift Reaction in Fuel Cell Applications. Part 1. Effect of the Support on the Reaction Sequence. *J. Catal.* **2007**, *251*, 153–162.
- (65) Panagiotopoulou, P.; Kondarides, D. I. Effect of the Nature of the Support on the Catalytic Performance of Noble Metal Catalysts for the Water-Gas Shift Reaction. *Catal. Today* **2006**, *112*, 49–52.
- (66) Gorte, R. J.; Zhao, S. Studies of the Water-Gas-Shift Reaction with Ceria-Supported Precious Metals. *Catal. Today* **2005**, *104*, 18–24.
- (67) Vignatti, C.; Avila, M. S.; Apesteguia, C. R.; Garetto, T. F. Catalytic and DRIFTS Study of the WGS Reaction on Pt-based Catalysts. *Int. J. Hydrogen Energy* **2010**, *35*, 7302–7312.
- (68) Phatak, A. A.; Koryabkina, N.; Rai, S.; Ratts, J. L.; Ruettiger, W.; Farrauto, R. J.; Blau, G. E.; Delgass, W. N.; Ribeiro, F. H. Kinetics of the Water-Gas Shift Reaction on Pt Catalysts Supported on Alumina and Ceria. *Catal. Today* **2007**, *123*, 224–234.
- (69) Roh, H. S.; Jeong, D. W.; Kim, K. S.; Eum, I. H.; Koo, K. Y.; Yoon, W. L. Single Stage Water-Gas Shift Reaction Over Supported Pt Catalysts. *Catal. Lett.* **2011**, *141*, 95–99.
- (70) Pazmino, J. H.; Shekhar, M.; Williams, W. D.; Akatay, M. C.; Miller, J. T.; Delgass, W. N.; Ribeiro, F. H. Metallic Pt as Active Sites for the Water-Gas Shift Reaction on Alkali-Promoted Supported Catalysts. *J. Catal.* **2012**, *286*, 279–286.
- (71) Xie, H.; Lu, J. L.; Shekhar, M.; Elam, J. W.; Delgass, W. N.; Ribeiro, F. H.; Weitz, E.; Poeppelmeier, K. R. Synthesis of Na-Stabilized Nonporous t-ZrO₂ Supports and Pt/t-ZrO₂ Catalysts and Application to Water-Gas-Shift Reaction. *ACS Catal.* **2013**, *3*, 61–73.
- (72) Wang, Y.; Zhai, Y. P.; Pierre, D.; Flytzani-Stephanopoulos, M. Silica-Encapsulated Platinum Catalysts for the Low-Temperature Water-Gas Shift Reaction. *Appl. Catal., B* **2012**, *127*, 342–350.
- (73) Kusche, M.; Bustillo, K.; Agel, F.; Wasserscheid, P. Highly Effective Pt-Based Water-Gas Shift Catalysts by Surface Modification with Alkali Hydroxide Salts. *ChemCatChem* **2015**, *7*, 766–775.
- (74) Kaidanovich, Z. V.; Kalishyn, Y. Y.; Grytsenko, V. I.; Kosmambetova, G. R.; Zyuzin, D. A.; Moroz, E. M.; Strizhak, P. E. Effect of the Carbon Support on the Catalytic Activity of Platinum Nanoparticles in the Water Gas Shift Reaction. *Theor. Exp. Chem.* **2015**, *S1*, 236–242.
- (75) Ding, K.; Gulec, A.; Johnson, A. M.; Schweitzer, N. M.; Stucky, G. D.; Marks, L. D.; Stair, P. C. Identification of Active Sites in CO Oxidation and Water-Gas Shift over Supported Pt Catalysts. *Science* **2015**, *350*, 189–192.
- (76) Mhadeshwar, A. B.; Vlachos, D. G. Microkinetic Modeling for Water-Promoted CO Oxidation, Water-Gas Shift, and Preferential Oxidation of CO on Pt. *J. Phys. Chem. B* **2004**, *108*, 15246–15258.
- (77) Gokhale, A. A.; Kandoi, S.; Greeley, J. P.; Mavrikakis, M.; Dumesic, J. A. Molecular-Level Descriptions of Surface Chemistry in Kinetic Models using Density Functional Theory. *Chem. Eng. Sci.* **2004**, *59*, 4679–4691.
- (78) Stamatakis, M.; Vlachos, D. G. A Graph-Theoretical Kinetic Monte Carlo Framework for On-Lattice Chemical Kinetics. *J. Chem. Phys.* **2011**, *134*, 214115.
- (79) Bollmann, L.; Ratts, J. L.; Joshi, A. M.; Williams, W. D.; Pazmino, J.; Joshi, Y. V.; Miller, J. T.; Kropf, A. J.; Delgass, W. N.; Ribeiro, F. H. Effect of Zn addition on the Water-Gas Shift Reaction over Supported Palladium Catalysts. *J. Catal.* **2008**, *257*, 43–54.
- (80) Vilekar, S. A.; Fishtik, I.; Datta, R. The Steady-State Kinetics of Parallel Reaction Networks. *Chem. Eng. Sci.* **2010**, *65*, 2921–2933.
- (81) Williams, W. D.; Greeley, J. P.; Delgass, W. N.; Ribeiro, F. H. Water Activation and Carbon Monoxide Coverage Effects on Maximum Rates for Low Temperature Water-Gas Shift Catalysis. *J. Catal.* **2017**, *347*, 197–204.
- (82) Bunluesin, T.; Gorte, R. J.; Graham, G. W. Studies of the Water-Gas-Shift Reaction on Ceria-Supported Pt, Pd, and Rh: Implications for Oxygen-Storage Properties. *Appl. Catal., B* **1998**, *15*, 107–114.
- (83) Jacobs, G.; Williams, L.; Graham, U.; Thomas, G. A.; Sparks, D. E.; Davis, B. H. Low Temperature Water-Gas Shift: in situ DRIFTS-Reaction Study of Ceria Surface Area on the Evolution of Formates on Pt/CeO₂ Fuel Processing Catalysts for Fuel Cell Applications. *Appl. Catal., A* **2003**, *252*, 107–118.
- (84) Iida, H.; Igarashi, A. Characterization of a Pt/TiO₂ (Rutile) Catalyst for Water Gas Shift Reaction at Low-Temperature. *Appl. Catal., A* **2006**, *298*, 152–160.
- (85) Panagiotopoulou, P.; Christodoulakis, A.; Kondarides, D. I.; Boghosian, S. Particle Size Effects on the Reducibility of Titanium Dioxide and its Relation to the Water-Gas Shift Activity of Pt/TiO₂ Catalysts. *J. Catal.* **2006**, *240*, 114–125.
- (86) Gonzalez, I. D.; Navarro, R. M.; Wen, W.; Marinkovic, N.; Rodriguez, J. A.; Rosa, F.; Fierro, J. L. G. A Comparative Study of the Water Gas Shift Reaction over Platinum Catalysts Supported on CeO₂, TiO₂ and Ce-modified TiO₂. *Catal. Today* **2010**, *149*, 372–379.
- (87) Bruix, A.; Rodriguez, J. A.; Ramirez, P. J.; Senanayake, S. D.; Evans, J.; Park, J. B.; Stacchiola, D.; Liu, P.; Hrbek, J.; Illas, F. A New Type of Strong Metal-Support Interaction and the Production of H₂ through the Transformation of Water on Pt/CeO₂(111) and Pt/CeO_x/TiO₂(110) Catalysts. *J. Am. Chem. Soc.* **2012**, *134*, 8968–8974.
- (88) Vecchietti, J.; Bonivardi, A.; Xu, W. Q.; Stacchiola, D.; Delgado, J. J.; Calatayud, M.; Collins, S. E. Understanding the Role of Oxygen Vacancies in the Water Gas Shift Reaction on Ceria-Supported Platinum Catalysts. *ACS Catal.* **2014**, *4*, 2088–2096.
- (89) Ganzler, A. M.; Casapu, M.; Maurer, F.; Stormer, H.; Gerthsen, D.; Ferre, G.; Vernoux, P.; Bornmann, B.; Frahm, R.; Murzin, V.; Nachtegaal, M.; Votsmeier, M.; Grunwaldt, J. D. Tuning the Pt/CeO₂ Interface by in Situ Variation of the Pt Particle Size. *ACS Catal.* **2018**, *8*, 4800–4811.
- (90) Lee, S. M.; Kim, G. J.; Lee, S. H.; Hwang, I. H.; Hong, S. C.; Kim, S. S. Catalytic Performance of Ce_{0.6}Y_{0.4}O₂-Supported Platinum Catalyst for Low-Temperature Water-Gas Shift Reaction. *ACS Omega* **2018**, *3*, 3156–3163.
- (91) Chen, Y.; Lin, J.; Li, L.; Qiao, B. T.; Liu, J. Y.; Su, Y.; Wang, X. D. Identifying Size Effects of Pt as Single Atoms and Nanoparticles Supported on FeO_x for the Water-Gas Shift Reaction. *ACS Catal.* **2018**, *8*, 859–868.
- (92) Jacobs, G.; Khalid, S.; Patterson, P. M.; Sparks, D. E.; Davis, B. H. Water-Gas Shift Catalysis: Kinetic Isotope Effect Identifies Surface Formates in Rate Limiting Step for Pt/Ceria Catalysts. *Appl. Catal., A* **2004**, *268*, 255–266.
- (93) Thimon, O.; Rachedi, K.; Diehl, F.; Avenier, P.; Schuurman, Y. Kinetics and Mechanism of the Water-Gas Shift Reaction Over Platinum Supported Catalysts. *Top. Catal.* **2009**, *S2*, 1940–1945.
- (94) Kalamaras, C. M.; Americanou, S.; Efsthathiou, A. M. “Redox” vs “Associative Formate with -OH Group Regeneration” WGS Reaction Mechanism on Pt/CeO₂: Effect of Platinum Particle Size. *J. Catal.* **2011**, *279*, 287–300.
- (95) Azzam, K. G.; Babich, I. V.; Seshan, K.; Lefferts, L. A Bifunctional Catalyst for the Single-Stage Water-Gas Shift Reaction in

- Fuel Cell Applications. Part 2. Roles of the Support and Promoter on Catalyst Activity and Stability. *J. Catal.* **2007**, *251*, 163–171.
- (96) Sabinis, K. D.; Akatay, M. C.; Cui, Y. R.; Sollberger, F. G.; Stach, E. A.; Miller, J. T.; Delgass, W. N.; Ribeiro, F. H. Probing the Active Sites for Water-Gas Shift over Pt/Molybdenum Carbide using Multi-Walled Carbon Nanotubes. *J. Catal.* **2015**, *330*, 442–451.
- (97) Schweitzer, N. M.; Schaidle, J. A.; Ezekoye, O. K.; Pan, X. Q.; Linic, S.; Thompson, L. T. High Activity Carbide Supported Catalysts for Water Gas Shift. *J. Am. Chem. Soc.* **2011**, *133*, 2378–2381.
- (98) Sabinis, K. D.; Cui, Y. R.; Akatay, M. C.; Shekhar, M.; Lee, W. S.; Miller, J. T.; Delgass, W. N.; Ribeiro, F. H. Water-Gas Shift Catalysis over Transition Metals Supported on Molybdenum Carbide. *J. Catal.* **2015**, *331*, 162–171.
- (99) Rodriguez, J. A.; Ramirez, P. J.; Gutierrez, R. A. Highly Active Pt/MoC and Pt/TiC Catalysts for the Low-Temperature Water-Gas Shift Reaction: Effects of the Carbide Metal/Carbon Ratio on the Catalyst Performance. *Catal. Today* **2017**, *289*, 47–52.
- (100) Osman, A. I.; Abu-Dahrieh, J. K.; Cherkasov, N.; Fernandez-Garcia, J.; Walker, D.; Walton, R. I.; Rooney, D. W.; Rebrov, E. A. Highly Active and Synergistic Pt/Mo₂C/Al₂O₃ Catalyst for Water-Gas Shift Reaction. *Mol. Catal.* **2018**, *455*, 38–47.
- (101) Zhang, X.; Shi, C.; Chen, B. B.; Kuhn, A. N.; Ma, D.; Yang, H. Progress in Hydrogen Production over Transition Metal Carbide Catalysts: Challenges and Opportunities. *Curr. Opin. Chem. Eng.* **2018**, *20*, 68–77.
- (102) Wang, Y.; Zhang, X. L.; Fu, Z. M.; Lu, Z. S.; Yang, Z. X. An Electronic Perturbation in TiC Supported Platinum Monolayer Catalyst for Enhancing Water-Gas Shift Performance: DFT study. *J. Phys.: Condens. Matter* **2019**, *31*, 305201.
- (103) Ammal, S. C.; Heyden, A. Water-Gas Shift Catalysis at Corner Atoms of Pt Clusters in Contact with a TiO₂ (110) Support Surface. *ACS Catal.* **2014**, *4*, 3654–3662.
- (104) Aranifard, S.; Ammal, S. C.; Heyden, A. On the Importance of the Associative Carboxyl Mechanism for the Water-Gas Shift Reaction at Pt/CeO₂ Interface Sites. *J. Phys. Chem. C* **2014**, *118*, 6314–6323.
- (105) Aranifard, S.; Ammal, S. C.; Heyden, A. On the Importance of Metal-Oxide Interface Sites for the Water-Gas Shift Reaction over Pt/CeO₂ Catalysts. *J. Catal.* **2014**, *309*, 314–324.
- (106) Nakamura, J.; Campbell, J. M.; Campbell, C. T. Kinetics and Mechanism of the Water-Gas Shift Reaction Catalyzed by the Clean and Cs-Promoted Cu(110) Surface—A Comparison with Cu(111). *J. Chem. Soc., Faraday Trans.* **1990**, *86*, 2725–2734.
- (107) Gokhale, A. A.; Dumescic, J. A.; Mavrikakis, M. On the Mechanism of Low-Temperature Water Gas Shift Reaction on Copper. *J. Am. Chem. Soc.* **2008**, *130*, 1402–1414.
- (108) Rodriguez, J. A.; Graciani, J.; Evans, J.; Park, J. B.; Yang, F.; Stacchiola, D.; Senanayake, S. D.; Ma, S. G.; Perez, M.; Liu, P.; Sanz, J. F.; Hrbek, J. Water-Gas Shift Reaction on a Highly Active Inverse CeO_x/Cu(111) Catalyst: Unique Role of Ceria Nanoparticles. *Angew. Chem., Int. Ed.* **2009**, *48*, 8047–8050.
- (109) Ammal, S. C.; Heyden, A. Nature of Pt-n/TiO₂(110) Interface under Water-Gas Shift Reaction Conditions: A Constrained ab Initio Thermodynamics Study. *J. Phys. Chem. C* **2011**, *115*, 19246–19259.
- (110) Aranifard, S.; Ammal, S. C.; Heyden, A. Nature of Pt-n/CeO₂
- (111) Surface under Water-Gas Shift Reaction Conditions: A Constrained ab Initio Thermodynamics Study. *J. Phys. Chem. C* **2012**, *116*, 9029–9042.
- (111) Flytzani-Stephanopoulos, M.; Gates, B. C. Atomically Dispersed Supported Metal Catalysts. *Annu. Rev. Chem. Biomol. Eng.* **2012**, *3*, 545–574.
- (112) Yang, X. F.; Wang, A. Q.; Qiao, B. T.; Li, J.; Liu, J. Y.; Zhang, T. Single-Atom Catalysts: A New Frontier in Heterogeneous Catalysis. *Acc. Chem. Res.* **2013**, *46*, 1740–1748.
- (113) Flytzani-Stephanopoulos, M. Gold Atoms Stabilized on Various Supports Catalyze the Water-Gas Shift Reaction. *Acc. Chem. Res.* **2014**, *47*, 783–792.
- (114) Liang, S. X.; Hao, C.; Shi, Y. T. The Power of Single-Atom Catalysis. *ChemCatChem* **2015**, *7*, 2559–2567.
- (115) Liu, J. Y. Catalysis by Supported Single Metal Atoms. *ACS Catal.* **2017**, *7*, 34–59.
- (116) Kim, J.; Kim, H. E.; Lee, H. Single-Atom Catalysts of Precious Metals for Electrochemical Reactions. *ChemSusChem* **2018**, *11*, 104–113.
- (117) Cui, X. J.; Li, W.; Ryabchuk, P.; Junge, K.; Beller, M. Bridging Homogeneous and Heterogeneous Catalysis by Heterogeneous Single-Metal-Site Catalysts. *Nat. Catal.* **2018**, *1*, 385–397.
- (118) Qiao, B. T.; Wang, A. Q.; Yang, X. F.; Allard, L. F.; Jiang, Z.; Cui, Y. T.; Liu, J. Y.; Li, J.; Zhang, T. Single-Atom Catalysis of CO Oxidation using Pt-1/FeO_x. *Nat. Chem.* **2011**, *3*, 634–641.
- (119) Gu, X. K.; Qiao, B. T.; Huang, C. Q.; Ding, W. C.; Sun, K. J.; Zhan, E. S.; Zhang, T.; Liu, J. Y.; Li, W. X. Supported Single Pt-1/Au-1 Atoms for Methanol Steam Reforming. *ACS Catal.* **2014**, *4*, 3886–3890.
- (120) Kinch, R. T.; Cabrera, C. R.; Ishikawa, Y. A Density-Functional Theory Study of the Water-Gas Shift Mechanism on Pt/Ceria(111). *J. Phys. Chem. C* **2009**, *113*, 9239–9250.
- (121) Peng, S. F.; Ho, J. J. The Adsorption and Dissociation of H₂O on TiO₂(110) and M/TiO₂(110) (M = Pt, Au) Surfaces-A Computational Investigation. *Int. J. Hydrogen Energy* **2010**, *35*, 1530–1536.
- (122) Bruix, A.; Lykhach, Y.; Matolinova, I.; Neitzel, A.; Skala, T.; Tsud, N.; Vorokhta, M.; Stetsovych, V.; Sevcikova, K.; Myslivecek, J.; Fiala, R.; Vaclavu, M.; Prince, K. C.; Bruyere, S.; Potin, V.; Illas, F.; Matolin, V.; Libuda, J.; Neyman, K. M. Maximum Noble-Metal Efficiency in Catalytic Materials: Atomically Dispersed Surface Platinum. *Angew. Chem., Int. Ed.* **2014**, *53*, 10525–10530.
- (123) Liang, J. X.; Lin, J.; Yang, X. F.; Wang, A. Q.; Qiao, B. T.; Liu, J. Y.; Zhang, T.; Li, J. Theoretical and Experimental Investigations on Single-Atom Catalysis: Ir-1/FeO_x for CO Oxidation. *J. Phys. Chem. C* **2014**, *118*, 21945–21951.
- (124) Zhang, R. Q.; Lee, T. H.; Yu, B. D.; Stampfl, C.; Soon, A. The Role of Titanium Nitride Supports for Single-Atom Platinum-Based Catalysts in Fuel Cell Technology. *Phys. Chem. Chem. Phys.* **2012**, *14*, 16552–16557.
- (125) Sen, F. G.; Qi, Y.; Alpas, A. T. Anchoring Platinum on Graphene using Metallic Adatoms: A First Principles Investigation. *J. Phys.: Condens. Matter* **2012**, *24*, 225003.
- (126) Poh, C. K.; Lim, S. H.; Lin, J. Y.; Feng, Y. P. Tungsten Carbide Supports for Single-Atom Platinum-Based Fuel-Cell Catalysts: First-Principles Study on the Metal-Support Interactions and O₂ Dissociation on WxC Low-Index Surfaces. *J. Phys. Chem. C* **2014**, *118*, 13525–13538.
- (127) Ding, W. C.; Gu, X. K.; Su, H. Y.; Li, W. X. Single Pd Atom Embedded in CeO₂(111) for NO Reduction with CO: A First-Principles Study. *J. Phys. Chem. C* **2014**, *118*, 12216–12223.
- (128) Hu, P. P.; Huang, Z. W.; Amghouz, Z.; Makkee, M.; Xu, F.; Kapteijn, F.; Dikhtarenko, A.; Chen, Y. X.; Gu, X.; Tang, X. F. Electronic Metal-Support Interactions in Single-Atom Catalysts. *Angew. Chem., Int. Ed.* **2014**, *53*, 3418–3421.
- (129) Li, F. Y.; Li, Y. F.; Zeng, X. C.; Chen, Z. F. Exploration of High-Performance Single-Atom Catalysts on Support M-1/FeO_x for CO Oxidation via Computational Study. *ACS Catal.* **2015**, *5*, 544–552.
- (130) Gao, G. P.; Jiao, Y.; Waclawik, E. R.; Du, A. J. Single Atom (Pd/Pt) Supported on Graphitic Carbon Nitride as an Efficient Photocatalyst for Visible-Light Reduction of Carbon Dioxide. *J. Am. Chem. Soc.* **2016**, *138*, 6292–6297.
- (131) Liu, X.; Yang, Y.; Chu, M. M.; Duan, T.; Meng, C. G.; Han, Y. Defect Stabilized Gold Atoms on Graphene as Potential Catalysts for Ethylene Epoxidation: A First-Principles Investigation. *Catal. Sci. Technol.* **2016**, *6*, 1632–1641.
- (132) Aleksandrov, H. A.; Neyman, K. M.; Vayssilov, G. N. The Structure and Stability of Reduced and Oxidized Mononuclear Platinum Species on Nanostructured Ceria from Density Functional Modeling. *Phys. Chem. Chem. Phys.* **2015**, *17*, 14551–14560.
- (133) Li, Q. H.; Ma, Z. J.; Sa, R. J.; Adidharma, H.; Gasem, K. A. M.; Russell, A. G.; Fan, M. H.; Wu, K. C. Computation-Predicted, Stable,

- and Inexpensive Single-Atom Nanocatalyst Pt@Mo₂C—An Important Advanced Material for H₂ Production. *J. Mater. Chem. A* **2017**, *5*, 14658–14672.
- (134) Wang, Y.; Zhang, X. L.; Cheng, C.; Yang, Z. X. TiC Supported Single-Atom Platinum Catalyst for CO Oxidation: A Density Functional Theory Study. *Appl. Surf. Sci.* **2018**, *453*, 159–165.
- (135) Thang, H. V.; Pacchioni, G.; DeRita, L.; Christopher, P. Nature of Stable Single Atom Pt Catalysts Dispersed on Anatase TiO₂. *J. Catal.* **2018**, *367*, 104–114.
- (136) Ammal, S. C.; Heyden, A. Titania-Supported Single-Atom Platinum Catalyst for Water-Gas Shift Reaction. *Chem. Ing. Tech.* **2017**, *89*, 1343–1349.
- (137) Ammal, S. C.; Heyden, A. Water-Gas Shift Activity of Atomically Dispersed Cationic Platinum versus Metallic Platinum Clusters on Titania Supports. *ACS Catal.* **2017**, *7*, 301–309.
- (138) Sharma, S.; Deshpande, P. A.; Hegde, M. S.; Madras, G. Nondeactivating Nanosized Ionic Catalysts for Water-Gas Shift Reaction. *Ind. Eng. Chem. Res.* **2009**, *48*, 6535–6543.
- (139) Deshpande, P. A.; Hegde, M. S.; Madras, G. A Mechanistic Model for the Water-Gas Shift Reaction over Noble Metal Substituted Ceria. *AIChE J.* **2009**, *56*, 1315–1324.
- (140) Zhai, Y. P.; Pierre, D.; Si, R.; Deng, W. L.; Ferrin, P.; Nilekar, A. U.; Peng, G. W.; Herron, J. A.; Bell, D. C.; Saltsburg, H.; Mavrikakis, M.; Flytzani-Stephanopoulos, M. Alkali-Stabilized Pt-OH_x Species Catalyze Low-Temperature Water-Gas Shift Reactions. *Science* **2010**, *329*, 1633–1636.
- (141) Yang, M.; Liu, J. L.; Lee, S.; Zugic, B.; Huang, J.; Allard, L. F.; Flytzani-Stephanopoulos, M. A Common Single-Site Pt(II)-O(OH)-(x)-Species Stabilized by Sodium on “Active” and “Inert” Supports Catalyzes the Water-Gas Shift Reaction. *J. Am. Chem. Soc.* **2015**, *137*, 3470–3473.
- (142) Zugic, B.; Bell, D. C.; Flytzani-Stephanopoulos, M. Activation of Carbon-Supported Platinum Catalysts by Sodium for the Low-Temperature Water-Gas Shift Reaction. *Appl. Catal., B* **2014**, *144*, 243–251.
- (143) Zugic, B.; Zhang, S. R.; Bell, D. C.; Tao, F.; Flytzani-Stephanopoulos, M. Probing the Low-Temperature Water-Gas Shift Activity of Alkali-Promoted Platinum Catalysts Stabilized on Carbon Supports. *J. Am. Chem. Soc.* **2014**, *136*, 3238–3245.
- (144) Moses-DeBusk, M.; Yoon, M.; Allard, L. F.; Mullins, D. R.; Wu, Z. L.; Yang, X. F.; Veith, G.; Stocks, G. M.; Narula, C. K. CO Oxidation on Supported Single Pt Atoms: Experimental and ab Initio Density Functional Studies of CO Interaction with Pt Atom on theta-Al₂O₃(010) Surface. *J. Am. Chem. Soc.* **2013**, *135*, 12634–12645.
- (145) Kistler, J. D.; Chotigkrai, N.; Xu, P. H.; Enderle, B.; Praserthdam, P.; Chen, C. Y.; Browning, N. D.; Gates, B. C. A Single-Site Platinum CO Oxidation Catalyst in Zeolite KLTL: Microscopic and Spectroscopic Determination of the Locations of the Platinum Atoms. *Angew. Chem., Int. Ed.* **2014**, *53*, 8904–8907.
- (146) Evin, H. N.; Jacobs, G.; Ruiz-Martinez, J.; Graham, U. M.; Dozier, A.; Thomas, G.; Davis, B. H. Low Temperature Water-Gas Shift/Methanol Steam Reforming: Alkali Doping to Facilitate the Scission of Formate and Methoxy C-H Bonds over Pt/Ceria Catalyst. *Catal. Lett.* **2008**, *122*, 9–19.
- (147) Evin, H. N.; Jacobs, G.; Ruiz-Martinez, J.; Thomas, G. A.; Davis, B. H. Low Temperature Water-Gas Shift: Alkali Doping to Facilitate Formate C-H Bond Cleaving Over Pt/Ceria Catalysts—An Optimization Problem. *Catal. Lett.* **2008**, *120*, 166–178.
- (148) Panagiotopoulou, P.; Kondarides, D. I. Effects of Alkali Promotion of TiO₂ on the Chemisorptive Properties and Water-Gas Shift Activity of Supported Noble Metal Catalysts. *J. Catal.* **2009**, *267*, 57–66.
- (149) Cybulskis, V. J.; Wang, J.; Pazmino, J. H.; Ribeiro, F. H.; Delgass, W. N. Isotopic Transient Studies of Sodium Promotion of Pt/Al₂O₃ for the Water-Gas Shift Reaction. *J. Catal.* **2016**, *339*, 163–172.
- (150) Kaftan, A.; Kusche, M.; Laurin, M.; Wasserscheid, P.; Libuda, J. KOH-Promoted Pt/Al₂O₃ Catalysts for Water Gas Shift and Methanol Steam Reforming: An Operando DRIFTS-MS Study. *Appl. Catal., B* **2017**, *201*, 169–181.
- (151) Faust, M.; Dinkel, M.; Bruns, M.; Bräse, S.; Seipenbusch, M. Support Effect on the Water Gas Shift Activity of Chemical Vapor Deposition-Tailored-Pt/TiO₂ Catalysts. *Ind. Eng. Chem. Res.* **2017**, *S6*, 3194–3203.
- (152) Sun, J. W.; Ruzsinszky, A.; Perdew, J. P. Strongly Constrained and Appropriately Normed Semilocal Density Functional. *Phys. Rev. Lett.* **2015**, *115*, 036402.
- (153) Sun, J. W.; Remsing, R. C.; Zhang, Y. B.; Sun, Z. R.; Ruzsinszky, A.; Peng, H. W.; Yang, Z. H.; Paul, A.; Waghmare, U.; Wu, X. F.; Klein, M. L.; Perdew, J. P. Accurate First-Principles Structures and Energies of Diversely Bonded Systems from an Efficient Density Functional. *Nat. Chem.* **2016**, *8*, 831–836.
- (154) Peterson, A. A.; Abild-Pedersen, F.; Studt, F.; Rossmeisl, J.; Norskov, J. K. How Copper Catalyzes the Electrocatalysis of Carbon Dioxide into Hydrocarbon Fuels. *Energy Environ. Sci.* **2010**, *3*, 1311–1315.
- (155) Medford, A. J.; Wellendorff, J.; Vojvodic, A.; Studt, F.; Abild-Pedersen, F.; Jacobsen, K. W.; Bligaard, T.; Norskov, J. K. Assessing the Reliability of Calculated Catalytic Ammonia Synthesis Rates. *Science* **2014**, *345*, 197–200.